Electronic Supplementary Material (ESI) for Energy & Environmental Science.

Operando Deconvolution of The Degradation Mechanisms of Iron-Nitrogen-Carbon Catalysts in Proton Exchange Membrane Fuel Cells

*Shiyang Liu[+], Quentin Meyer[+], Chen Jia, Shuhao Wang, Chengli Rong, Yan Nie, and Chuan Zhao**

School of Chemistry, The University of New South Wales, Sydney, NSW, 2052, Australia

*Corresponding author: chuan.zhao@unsw.edu.au
[+]Authors contributed equally.

Supplementary Information

Contents

1. Methods

Chemicals

2-Methylimidazole (99%), iron(III) chloride hexahydrate, zinc nitrate hexahydrate, and perfluorinated resin solution containing Nafion (5 wt. %) were purchased from Sigma-Aldrich, iso-propyl-alcohol and methanol were purchased from ChemSupply, sulfuric acid (98%) was purchased from Merck. All chemicals are used as received. All gases were purchased from Coregas, using a purity of 99.995%. All gases were purchased from Coregas, using a purity of 99.995%.

Catalyst synthesis

5.88 g Zn $(NO_3)_2 \cdot 6H_2O$ was dissolved in 200 mL methanol and 6.48g 2MIm was dissolved in another 200 mL methanol. These two solutions were mixed and stirred for 150 min at room temperature. Following the reaction, the white sediments were collected via centrifugation and washed three times with methanol and finally dried under a vacuum at 60 °C overnight. Nitrogen-doped porous carbon (N-C host) was obtained by heating ZIF-8 in a tube furnace at 1000 °C under an N_2 atmosphere for an hour. 30 mg of the N-C host was dispersed in 20 mL deionized water, followed by an hour of ultrasonic treatment to form a homogeneous suspension. 0.100 mL of 0.1 M $FeCl_3 \cdot 6H_2O$ was then added to the above solution with the resulting dispersion stirred for an hour. The mixture was then heated and stirred for 2 hours in an oil bath (70 °C). The resulting solution was dried on a hot plate at 200 °C, with the collection of the Fe^{3+}-doped N-C host powder. The final Fe-N-C was obtained by pyrolyzing the Fe^{3+} doped N-C host at 1000 °C under an Ar atmosphere for two hours with a heating rate of 10 °C min^{-1}. A magnet was used to remove catalysts that may contain any Fe nanoparticles. The catalyst ink was prepared by mixing 10 mg catalyst with 0.230 mL of 5 wt% Nafion solution (Aldrich), 0.885 mL of 2-propanol, and 0.885 mL of deionized water

Half-cell testing

Half-cell testing was conducted on a rotating ring disk electrode (RRDE, Pine Research Instrumentation) with an electrochemical workstation (CHI760E, CH Instruments) in 0.5 M H_2SO_4 solution at room temperature. All potentials reported in this study were calibrated to the reversible hydrogen electrode. The counter electrode was a graphite rod, the reference electrode was a saturated calomel electrode, and a glassy carbon disk (ϕ=5mm) coated with catalyst inked as the working electrode. The obtained mixture was sonicated for one hour and stirred for 30 mins to form a homogeneous ink. For all half-cell testing, the loading of the N-C and Fe-N-C catalysts are 600 μg cm^{-2} and 60 μg $_{pt}$ cm^{-2} for Pt/C (20 wt%). The electrolyte was purged with either Ar or O_2 for 30 minutes before tests. The linear sweep voltammetry current was obtained by subtracting the background current measured in an Ar-saturated electrolyte

from the current measured in an oxygen-saturated electrolyte. The hydrogen peroxide yield (H_2O_2%) was calculated as follows:

$$H_2O_2\% = \frac{200\, I_r}{N|I_d| + I_r} \quad (1)$$

Where *N* is the current collection efficiency of the Pt ring (43.9%), I_r is the ring current, and I_d is the disk current of the RRDE. The electron transfer number, *n*, was calculated as follows:

$$n = \frac{4|I_d|}{|I_d| + I_r/N} \quad (2)$$

The methanol poisoning test was conducted by injecting methanol solution into the electrolyte during a chronoamperometric test at 0.5 V against the reversible hydrogen electrode. The stability of the catalyst was assessed by applying a constant voltage at 0.5 V against the reversible hydrogen electrode at 200 rpm for 10,000 s, the current was recorded after stabilization.

Fuel cell testing

The catalyst ink was drop-casted on a 1 cm^2 commercial gas diffusion layer with a microporous layer (Sigracet 36BB, FuelCellStore), and dried on a hot plate for 30 minutes at 100 °C to create a gas diffusion electrode. The loading was 3 mg cm^{-2} for the Fe-N-C cathode and 0.2 mg_{Pt} cm^{-2} for the Pt/C cathode. A commercial gas diffusion electrode with a 0.2 mg_{Pt} cm^{-2} Pt loading was used as an anode. To fabricate the membrane electrode assembly, a piece of Nafion 211 membrane (FuelCellStore, US) was sandwiched between the anode and as-prepared cathode and hot-pressed at 130 °C for 90 s under 2 bar absolute pressure. A commercial fuel cell tester (850e, Scribner) was used for single-cell testing with a flow rate of 0.1 L min^{-1} for H_2 and 0.4 L min^{-1} for O_2/air, respectively. All gases used were 100% humified, with the cell and gases heated to 80 °C. A modified stability test was conducted on the Fe-N-C cathode PEMFC at 1 A cm^{-2} for 60 hours with 2.5 bar absolute pressure with polarizations, impedance spectroscopy and cyclic voltammetry after 0, 0.5, 1, 1.5, 2, 3, 5, 10, 15, 20, 25, 30, 40, 50 and 60 hours.

H_2O_2 production and accumulation in PEMFC over time

The cumulative number of mol of H_2O_2 produced in PEMFC after 60 hours at 1 A cm^{-2} is calculated as follows[1]:

The number of mol of H_2O_2 per mol of electrons, R_1, is calculated as follows:

$$R_1 = \frac{x}{\left(100 n_e(H_2O) - x n_e(H_2O_2)\right)} \quad (3)$$

With $n_e(H_2O)$ the number of electrons for the 4-electron pathway and $n_e(H_2O_2)$ the number of electrons for the 2-electrons pathway, and *x* the hydrogen peroxide yield (%).

The number of mol of electrons per mg of catalyst, R_2, is calculated as follows:

$$R_2 = \frac{I\Delta t}{FL} \quad (4)$$

With *I* the applied current, Δt the experiment duration, *F* Faraday constant, and *L* the catalytic loading.

As a result, the cumulative number of mol of H_2O_2 per mg of catalyst is calculated as:

$$N_{H_2O_2} = R_1 R_2 \quad (5)$$

Cyclic voltammetry

Cyclic voltammetry was performed in 0.1 L min^{-1} H_2/ 2 L min^{-1} N_2 from 0.05 V to 1 V with a scan rate of 50 mV s^{-1} to use the anode as a pseudo-reference electrode. Before the cyclic voltammetry, the cell was left for 30 mins at open circuit voltage in H_2/N_2, followed by 15 mins at 0.1 V in H_2/N_2 to ensure that any remaining O_2 has been consumed. Voigt deconvolution using the Matlab® software *DCscript* was used to separate the two overlapping peaks between 0.6 V and 0.8 V and calculate their induvial area (charge) with background subtraction to remove the influence of the capacitance[2]. The double layer capacitance was obtained from cyclic voltammetry, using the following equation[3]:

$$C_{dl} = \frac{\left(i_{cv,+}^{0.3V} + \left|i_{cv,-}^{0.3V}\right|\right)}{2\nu} \quad (6)$$

where ν is the scan rate (50 mV s^{-1}) and $i_{cv,+}^{0.3V}$ and $i_{cv,-}^{0.3V}$ are the current densities measured at 0.3 V in respectively the positive and negative scans.

Polarizations

Polarizations were captured in H_2/O_2 with increments of 12.5 mA cm^{-2} lasting 5 s below 100 mA cm^{-2} and 100 mA cm^{-2} above 100 mA cm^{-2}. These were interrupted for voltages below 0.2 V. The catalytic activity was measured at 0.8 $V_{iR\text{-}free}$.

Electrochemical impedance spectroscopy

Electrochemical impedance spectroscopy was performed at 1 A cm^{-2}, with 30 s stabilization time before the impedance measurement. A frequency range from 5 kHz to 0.1 Hz was used with 10 frequencies per decade, 12.5% amplitude, with an integration time of 1s and 3 integration cycles. These settings were used to minimize the signal-to-noise ratio. The electrochemical impedance was analysed using the distribution of relaxation times (DRT). DRT is evaluated from the impedance Z data using equation (7).

$$Z(f) = R_{\infty} + R_{pol}\int_{0}^{\infty} \frac{g(\tau)}{1 + 2i\pi f\tau} d\tau \quad (7)$$

Where R_{∞} is the ohmic resistance, R_{pol} is the polarization resistance, g is the DRT function, τ is the relaxation time and f is the frequency[4, 5]. The Matlab® software *DRTtools* developed by the Ciucci group was used to calculate the DRT function[4, 5]. A well-chosen regularization parameter λ is necessary to determine the DRT function from the discrete impedance dataset with 10 frequencies per decade in logarithmic decrement to the pseudo-continuous time domain of the DRT function. A regularization parameter λ of 10^{-3} was used following Heinzmann's study, as it represents an excellent trade-off between low-residuals, selectivity and minimal oscillations for PEMFCs[6]. Voigt deconvolution without background subtraction using the Matlab® software *DCscript* was used to separate individual peaks, detect the peak maximum frequency and calculate the intensity of each peak under the logarithmic scale (resistance)[2]. The highest frequency of each peak is used as a representation of the rate of the allocated process (in Hz, or s^{-1}), while the integrated peak area corresponds to its resistance[2, 7].

Physical characterization

Scanning electron microscopy (SEM, JEOL 7001F) and transmission electron microscopy (TEM, JEOL F200) accompanied by high-resolution transmission electron microscopy (HR-TEM) was employed to study the catalysts. Transmission electron microscopy (TEM, JEOL F200) accompanied by high-resolution transmission electron microscopy (HR-TEM) was employed to study the catalysts in membrane electrode assembly before operations and after 60 hours of operations, by removing the cathode gas diffusion electrode from the membrane and scratching off small amounts of catalyst powder. The high-angle annular dark field (HAADF) was acquired using an FEI Themis-Z image, monochromated, and probe-corrected 60-300 kV STEM (Thermo Fisher, US). X-ray diffraction (XRD, Aeris, PANalytical) and X-ray photoelectron spectroscopy (XPS, Thermo ESCALAB250i) were applied to investigate crystal structures and chemical compositions. Raman spectra were obtained using a Renishaw INVIA micro-Raman spectroscopy system with a laser excitation of 532 nm. Inductively coupled plasma mass spectrometry (ICP-MS, PerkinElmer) was applied to investigate the membrane electrode assembly composition by diluting a small portion (~0.2 cm^2) of a membrane electrode assembly in concentrated nitric acid solution before PEMFC operations, and after 1 hour and 60 hours of operations, and to probe the accumulated water F^- concentration after 60 hours of operation. The equipment's lower detection limit is 100 ppm.

X-ray computed tomography

Laboratory X-ray computed tomography system (Mark I Heliscan™ microCT, ThermoFisher, USA) was used for 3D imaging of the membrane electrode assembly before and after 60 hours. 2 mm diameter samples were extracted from the 1 cm^2 membrane electrode assembly to

optimize the image collection process and maximize the signal-to-noise ratio. A source voltage and current of 60 kV and 190 µA were used for every sample. The sample was rotated over a 360° axis using 2,880 projections, with a 6 s exposure and 5 accumulations. The two samples were placed between 2.2 and 2.8 mm from the source, which resulted in 0.9 – 1.2 µm/pixel depending on the sample. A field-of-view of 500 µm × 500 µm, larger than the representative elementary area of 0.1 mm^2 in the *x-y* orientation[8] was chosen for material segmentation. The 3D orthoslices were segmented using Avizo (FEI) to separate the Nafion membrane from the gas diffusion layer, anode, and cathode catalyst layers (*Segmentation toolkit,* Avizo). The roughness of the Fe-N-C cathode, *r* (membrane facing side), was calculated as follows[8]:

$$r = \frac{A_{act}}{A_{slice}} \tag{8}$$

A_{act} is the outer surface area of the catalyst layer in contact with the membrane, and A_{slice} is the geometric surface area of a single slice.

X-ray Absorption Spectroscopy

Fe K-edge XAS spectra were recorded on the XAS beamline 12 ID at the Australian Synchrotron, ANSTO in Clayton, Victoria. The excitation energy was selected with a double-crystal Si (111) monochromator with focusing optics. Energy calibration of the monochromator was performed at the Fe-K absorption edge with an inline Fe metal foil (first maximum of the first derivative at 7110.75 eV). Powder samples of Fe-N-C catalysts and of Fe(II)Pc were mixed with cellulose and pelletized as 7 mm diameter disks. Measurements of the Fe-N-C catalyst were also performed in membrane electrode assembly, using either fresh samples or samples following 10 and 60 hours of operations at 1 A cm^{-2} with the samples vacuum sealed after completing cell operations. All samples were performed in fluorescence mode using a 100-element solid-state HP-Ge detector (Canberra/Mirion, France) due to the low Fe content (2.09 at%, XPS). All XANES results were processed using the Athena® software.

Theoretical modelling

Density functional theory (DFT) and ab initio molecular dynamic (AIMD) were employed to investigate the stability of catalysts using the QUANTUM ESPRESSO 7.1 code[9]. The relaxation of geometries was conducted at the generalized gradient approximation (GGA) level[10]. Ultra-soft pseudopotentials and the revised Perdew-Burke-Ernzerhof functional (RPBE) were utilized.[11] Spin-polarized calculations were carried out, achieving optimal convergence with plane-wave and density cutoffs of 50 and 500 Ry, respectively. respectively. A Fermi-level smearing width of 0.1 eV was applied. AIMD simulations were performed in the canonical ensemble (NVT) using the Nose-Hoover thermostat method at a temperature of 300 K for a duration of 2 ps, with a timestep of 0.9676 fs[12]. To reduce computational costs, the hydrogen

mass was increased to 2 atomic mass units (H/D-exchange). The functionalized graphene structure was modelled in a 4 × 4 fully optimized unit cell with periodic boundary conditions. A vacuum region of at least 15 Å was incorporated to prevent interactions between periodic images. In this model, two carbon atoms were removed, and four carbon atoms surrounding the divacancy were replaced, resulting in the formation of a double-vacancy four-nitrogen-doped graphene[13]. An iron atom was subsequently added at the centre of the nitrogen site (see **Fig. S14a**). Monkhorst-Pack k-point grids of 3 × 3 × 1 were employed. Further optimization was performed on Fe-N_4/graphene catalysts with dominant reactive intermediates adsorbed on Fe sites (*FeOH, HO*FeOH, and *$Fe(OH)_2$) (**Fig. S14b-d**). Subsequently, two adsorbed hydrogen atoms on the nitrogen sites of Fe-N_4/graphene catalysts were optimized using static DFT, and the resulting geometries are depicted **in Fig. S14e-f**. AIMD simulations were employed to investigate the changes in Fe-N bonds under dynamic condition, and atomic coordinates were obtained at different time intervals (**Fig. S15**). The internal energy of various intermediates during AIMD simulations is presented in **Fig. S16** to confirm the convergence of simulation.

2. Supplementary Figures and Tables

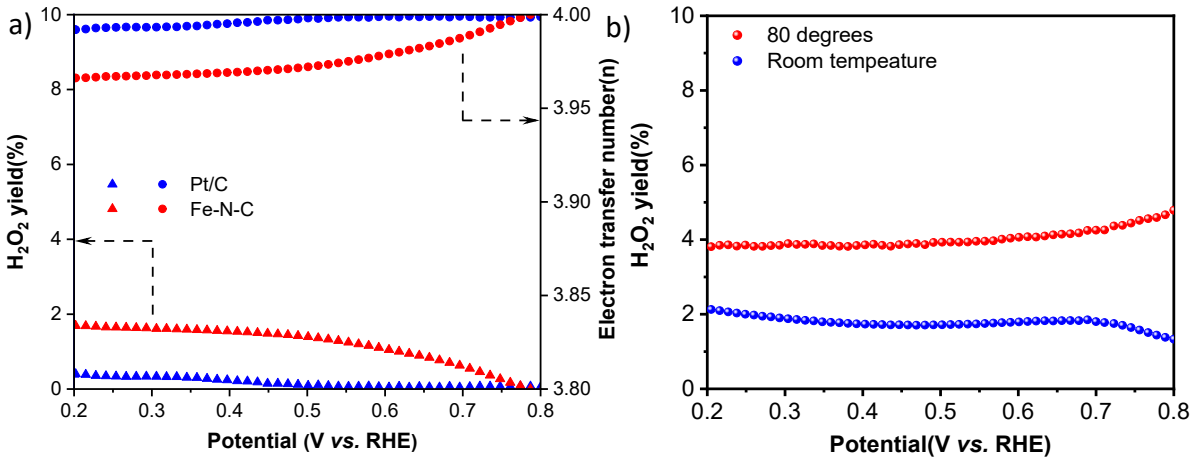

Supplementary Fig. 1 a) Hydrogen peroxide yield and electron transfer number of Pt/C and Fe-N-C catalysts at ambient temperature. b) Hydrogen peroxide yield of Fe-N-C catalysts at ambient and 80 °C.

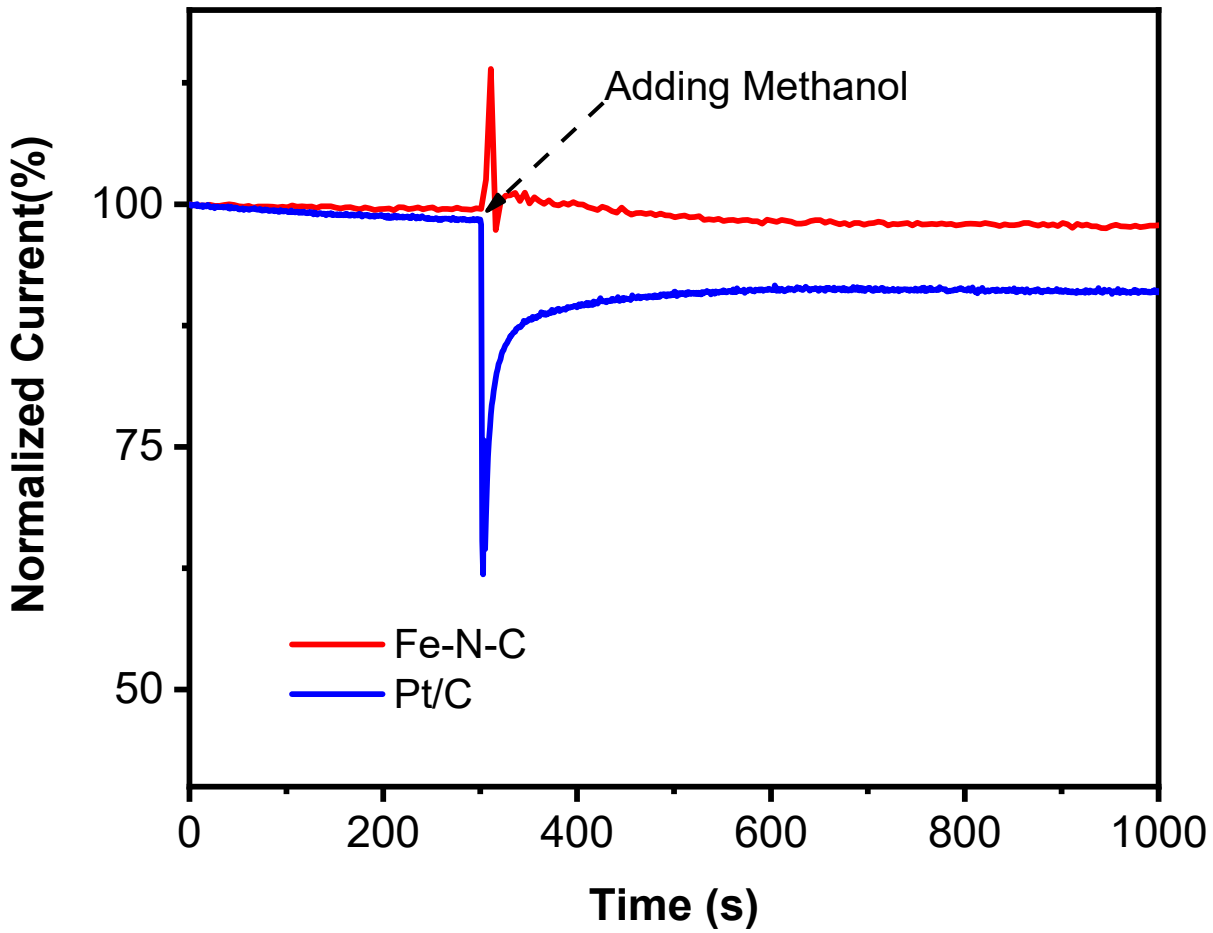

Supplementary Fig. 2 Methanol tolerance evaluation of Pt/C and Fe-N-C catalyst by chronoamperometry at 0.5 V and adding methanol around 300 s.

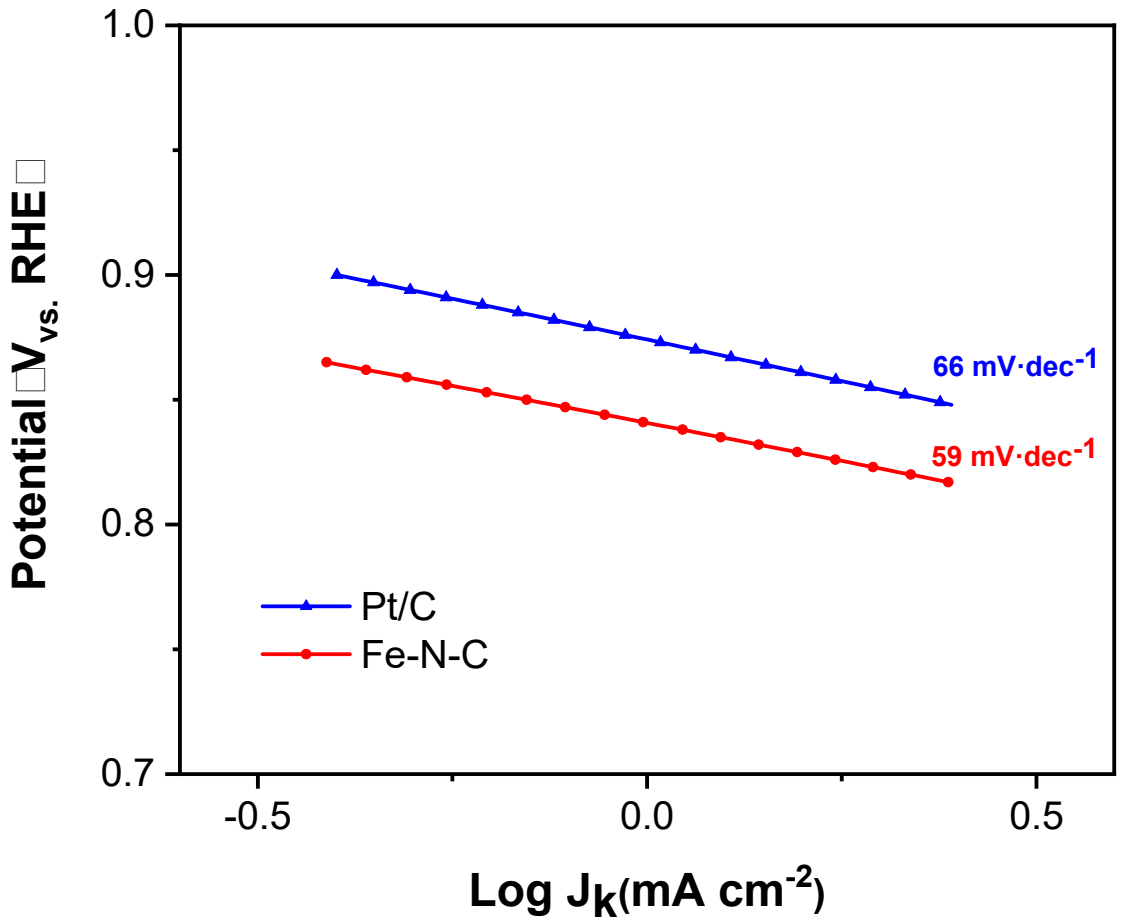

Supplementary Fig. 3 Tafel plots of Pt-C and Fe-N-C catalyst.

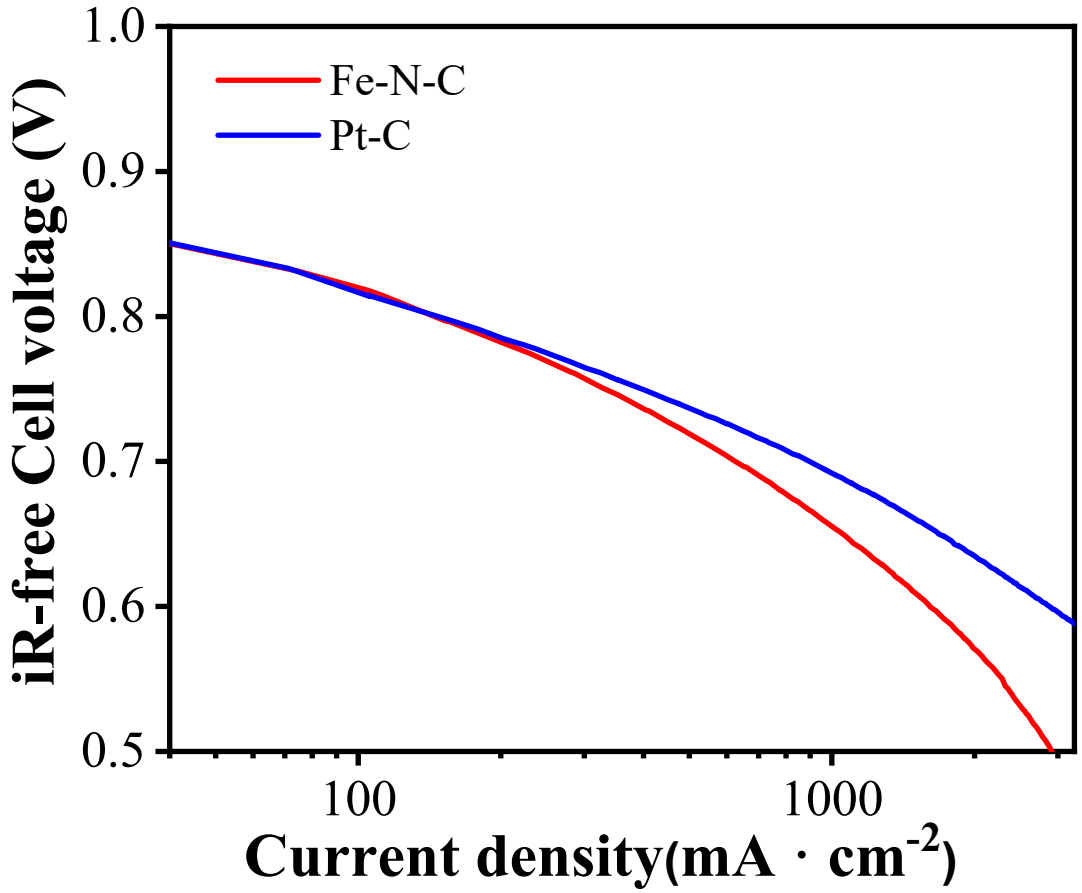

Supplementary Fig. 4 Tafel plots of the iR-free polarization curves for membrane electrode assemblies using Pt/C and Fe-N-C cathodes at the beginning of life.

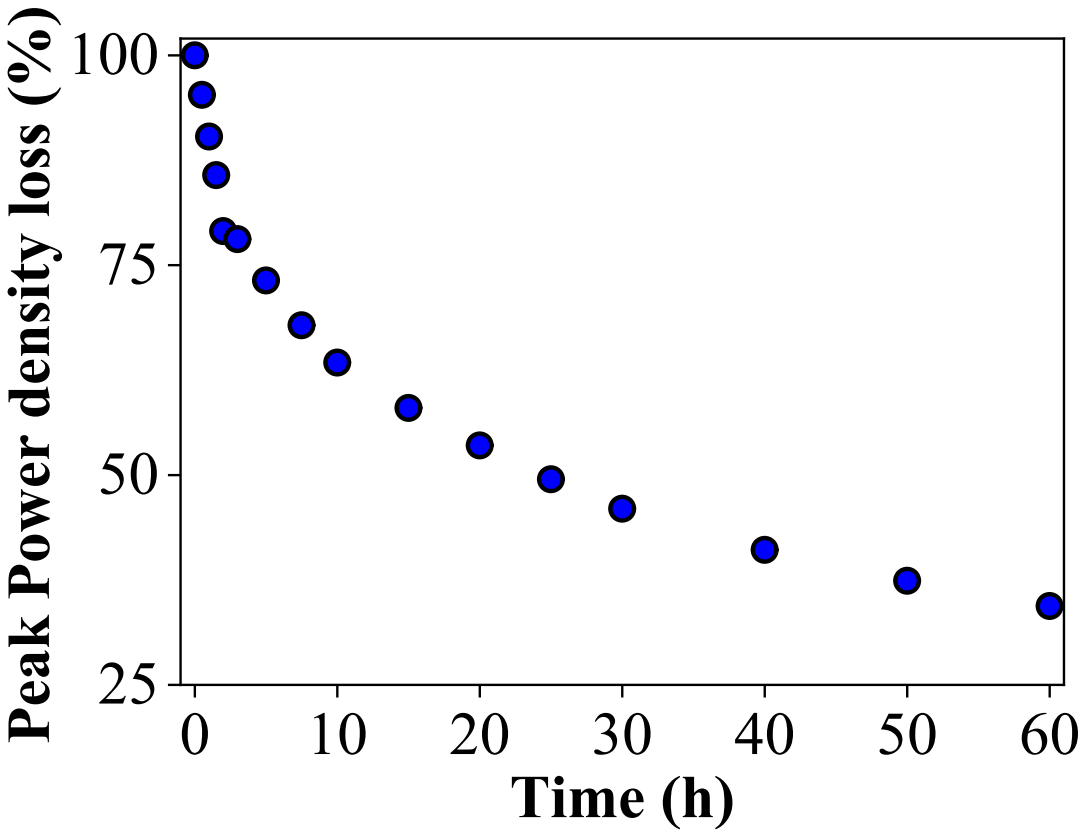

Supplementary Fig. 5 Peak power density loss of Fe-N-C PEMFC over the 60 hours stability test.

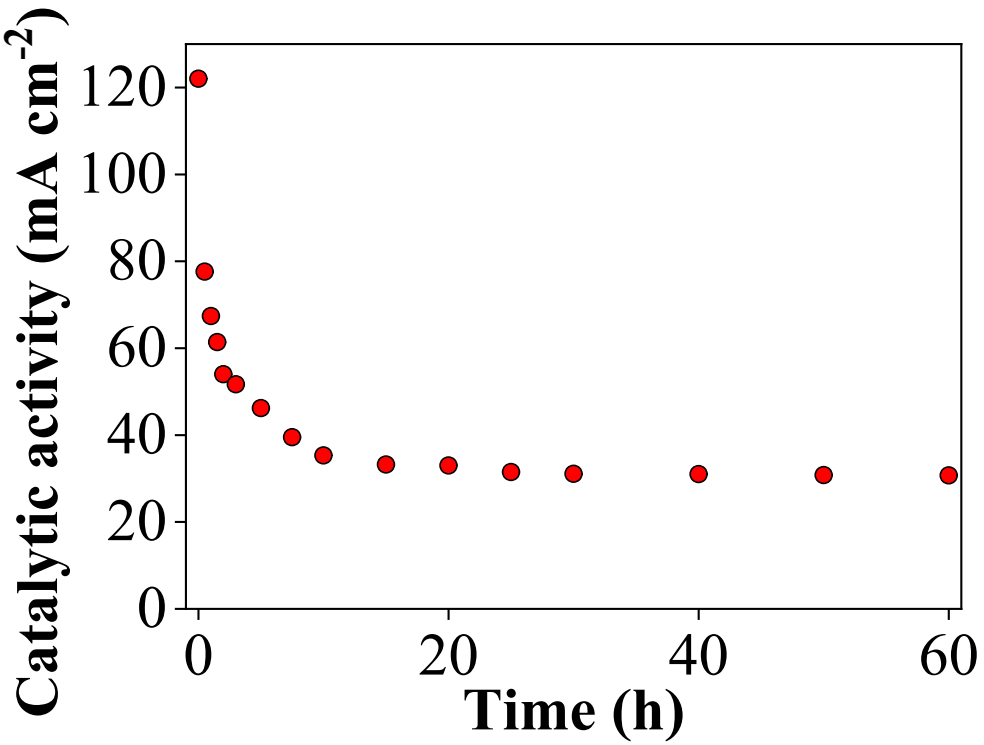

Supplementary Fig. 6 Catalytic activity obtained at 0.8 V (iR-free).

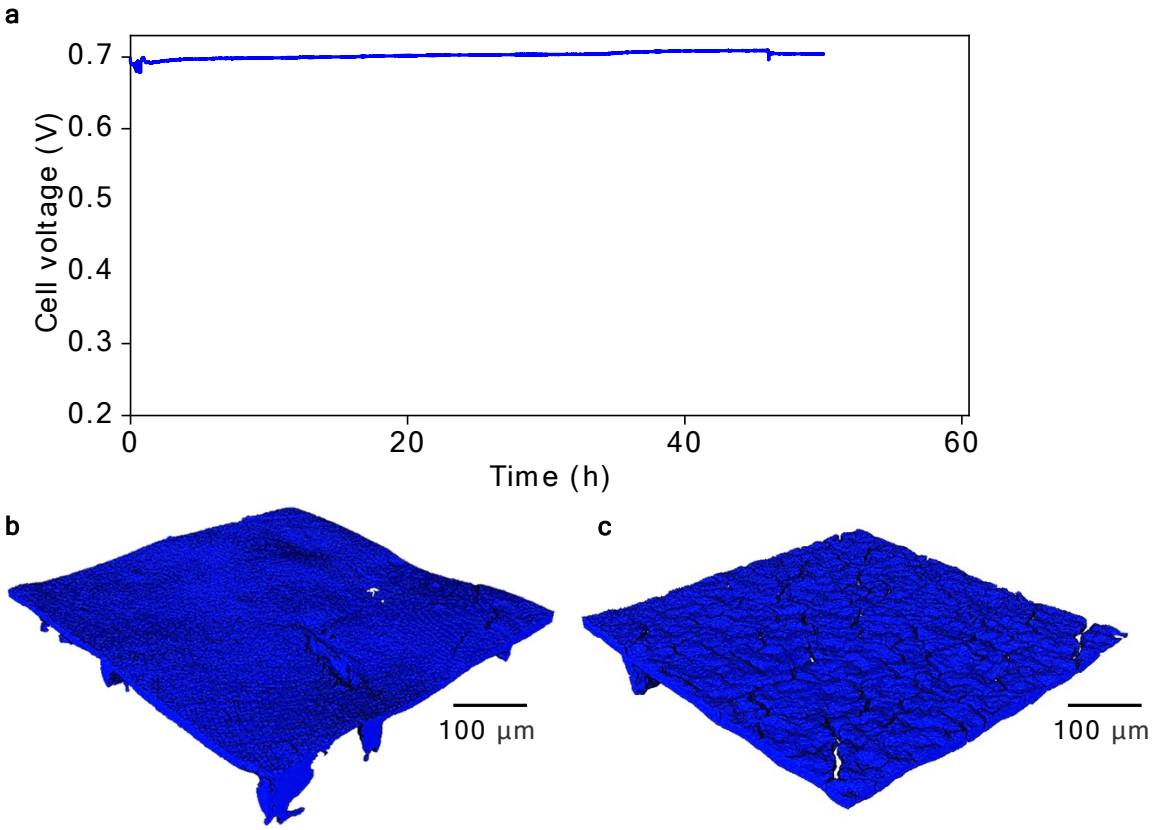

Supplementary Fig. 7 a Stability of Pt/C catalysts in PEMFC s over 60 at 1 A cm^{-2} at 80 ^{o}C with 2.5 bar absolute pressure at fully humidified O_2 and H_2 with flow rates of 0.1 L min^{-1} and 0.4 L min^{-1}, and **b** cathode catalyst layer structure b) before and c) after 60 hours.

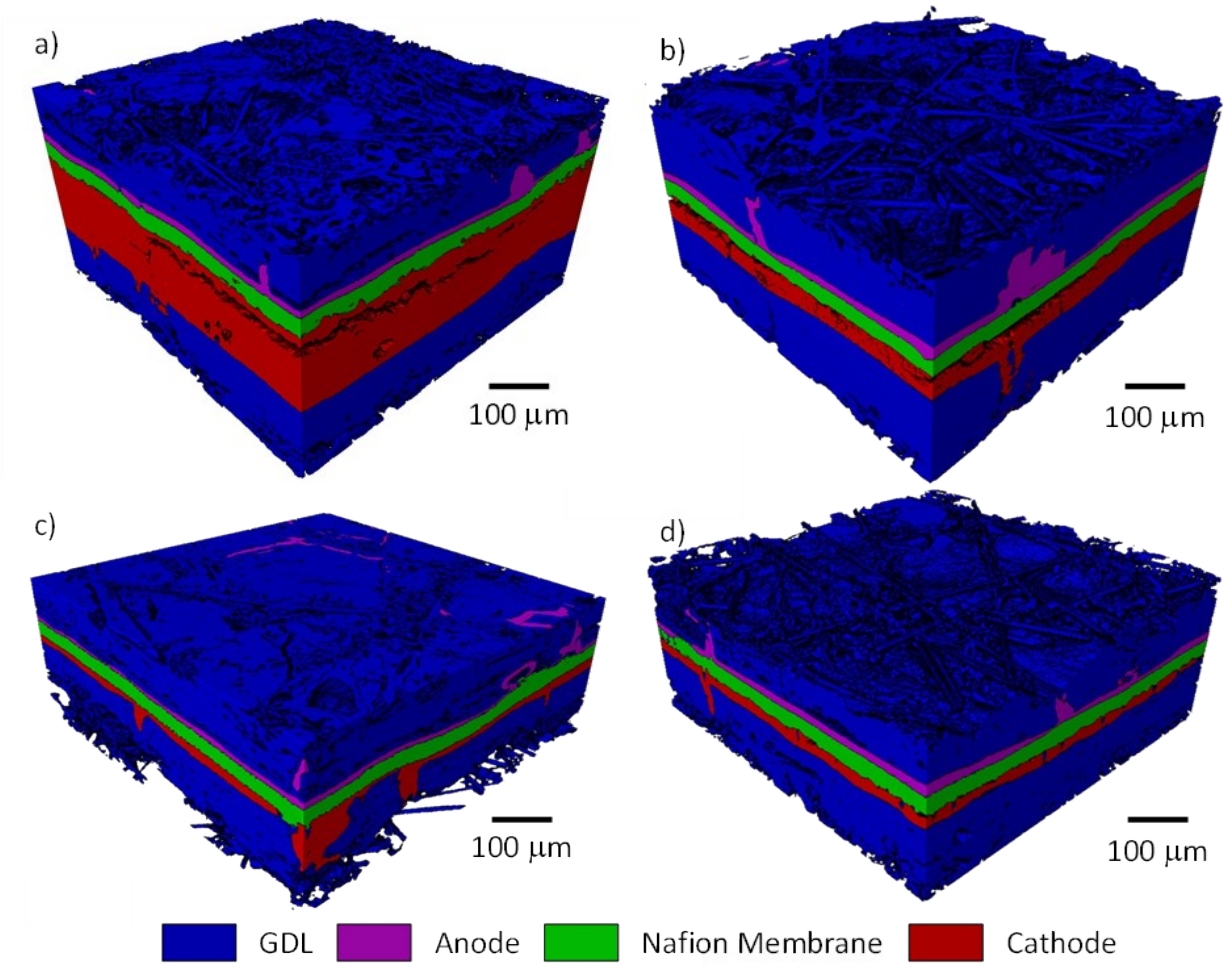

Supplementary Fig. 8 3-D volume rendering of membrane electrode assembly from X-CT, with **a** fresh Fe-N-C, **b** 60h Fe-N-C, **c** Fresh Pt/C and d) 60h Pt/C.

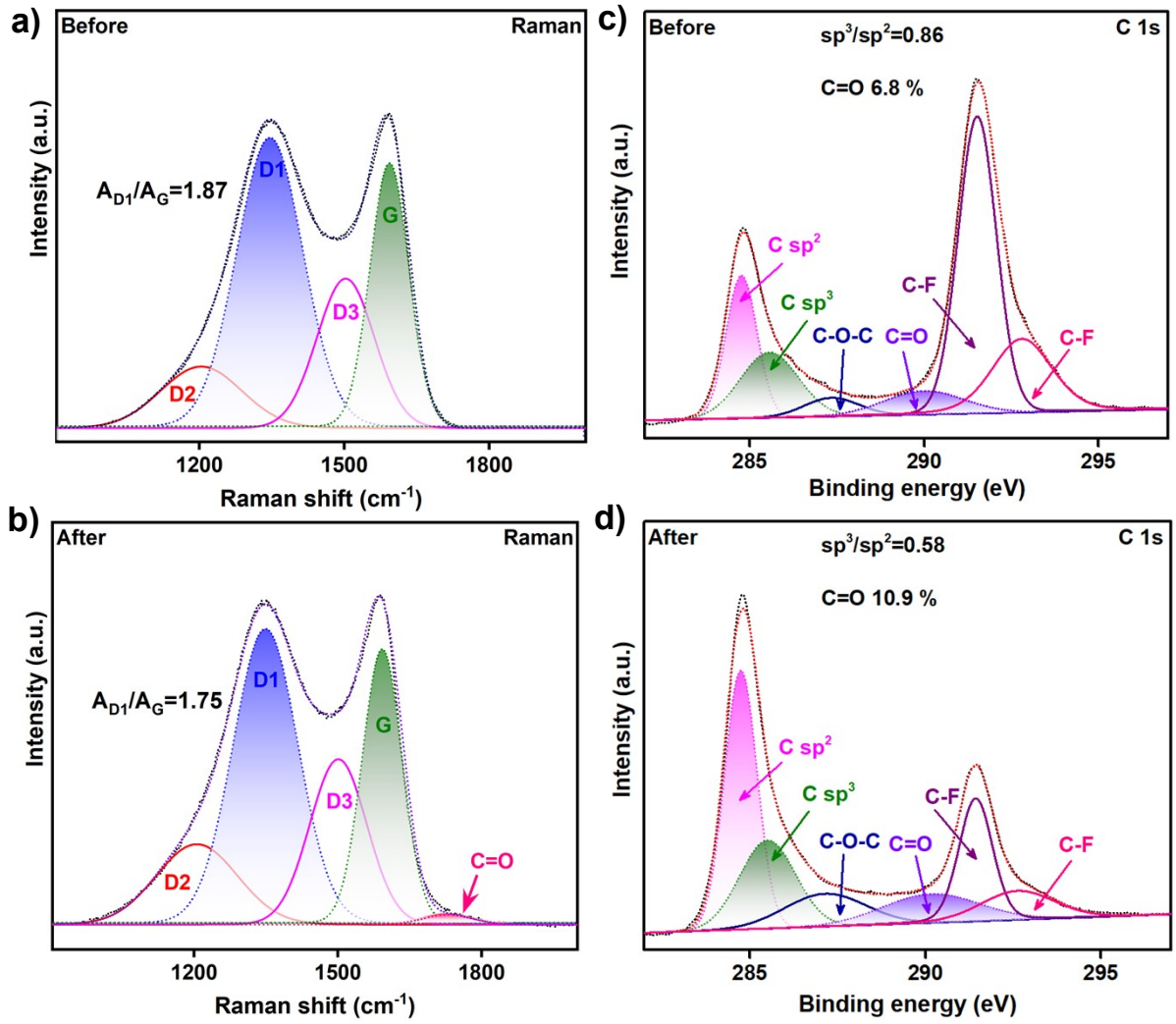

Supplementary Figure 9. a, b) Raman spectra and c, d) high-resolution C 1s spectrum for the catalyst before and after the test.

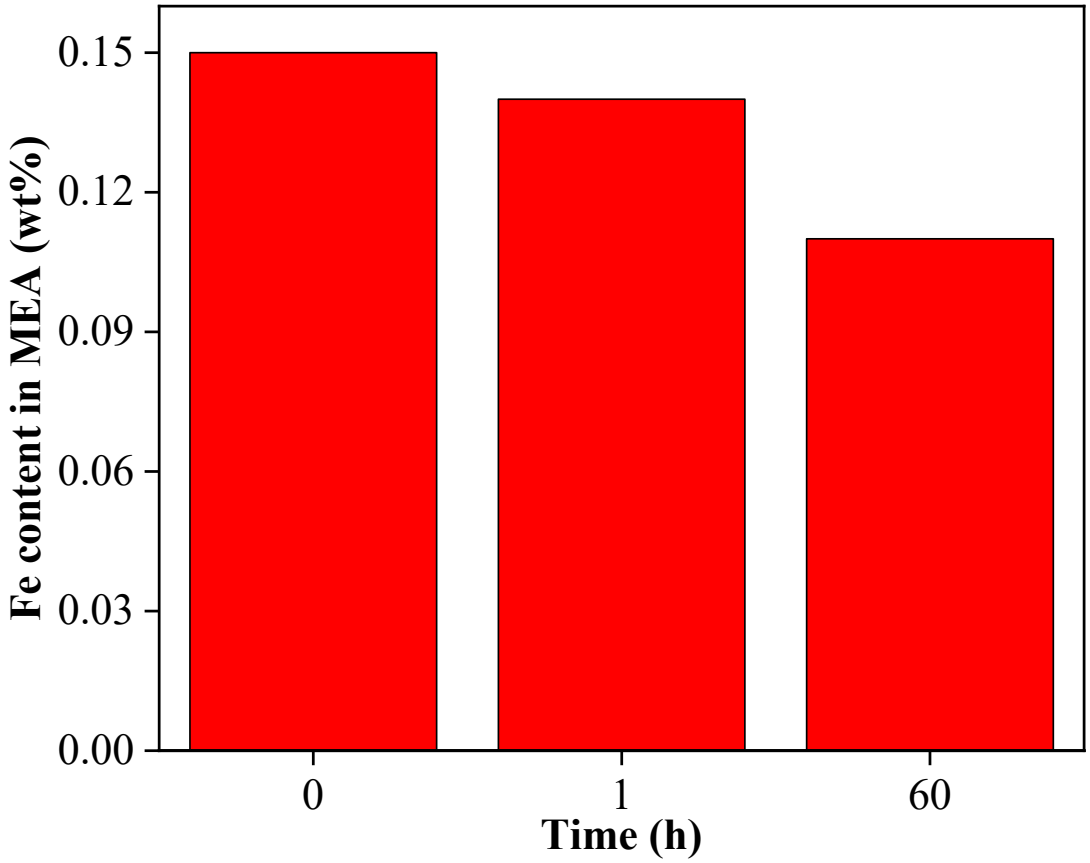

Supplementary Fig. 10 ICP results of 0.2 mm^2 of membrane electrode assemblies before the test and after 1 h and 60 h at 1 A cm^{-2}.

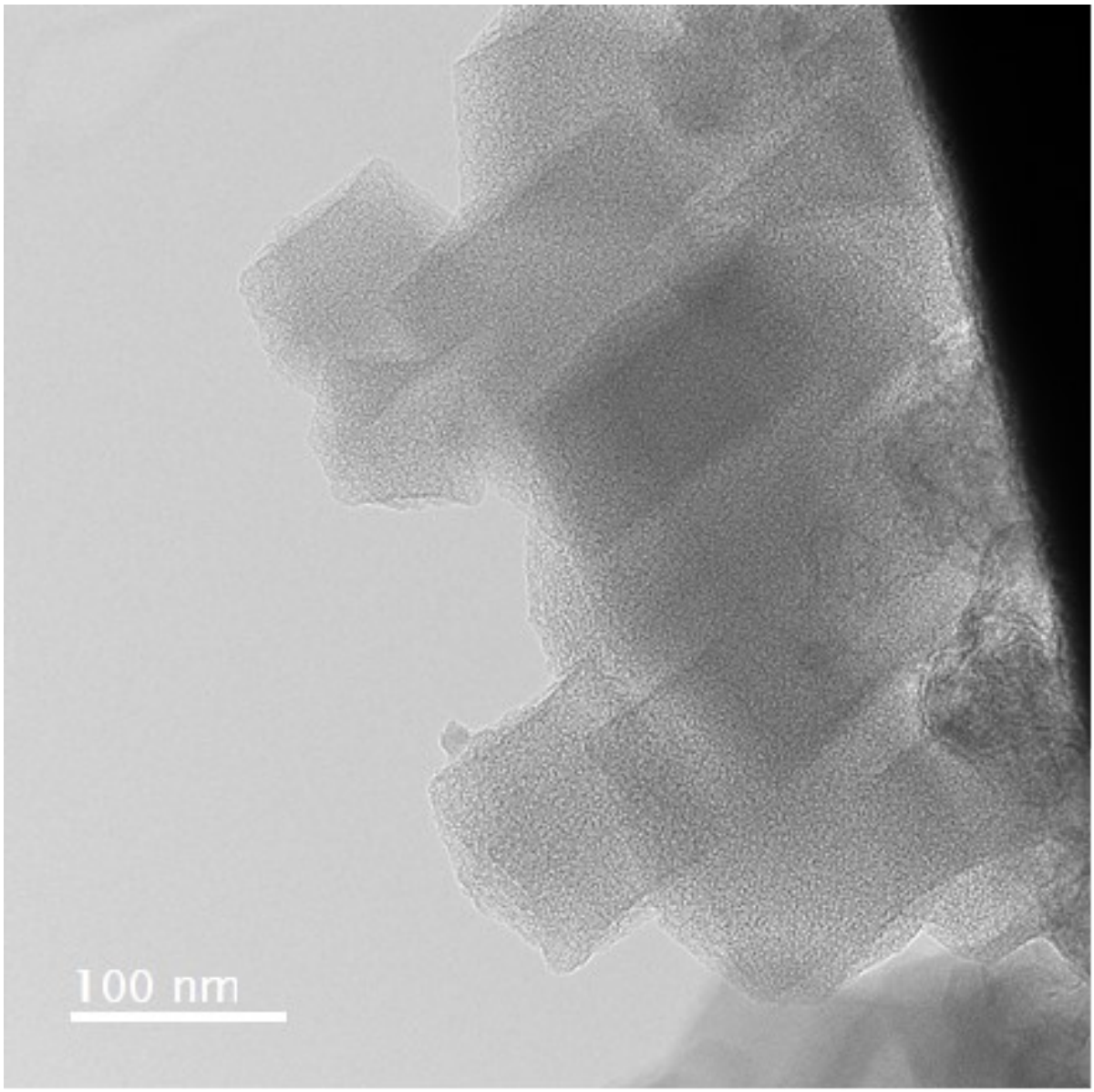

Supplementary Fig. 11 TEM images of Fe-N-C catalyst from untested membrane electrode assembly.

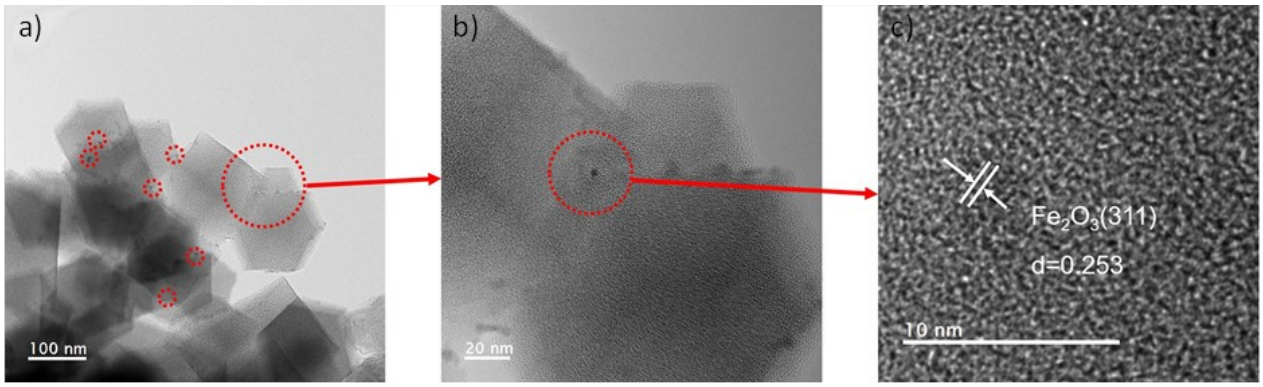

Supplementary Fig. 12 a-b TEM and **c** HR-TEM of Fe-N-C following 60 hours of operations in the membrane electrode assembly at 1 A cm^{-2}.

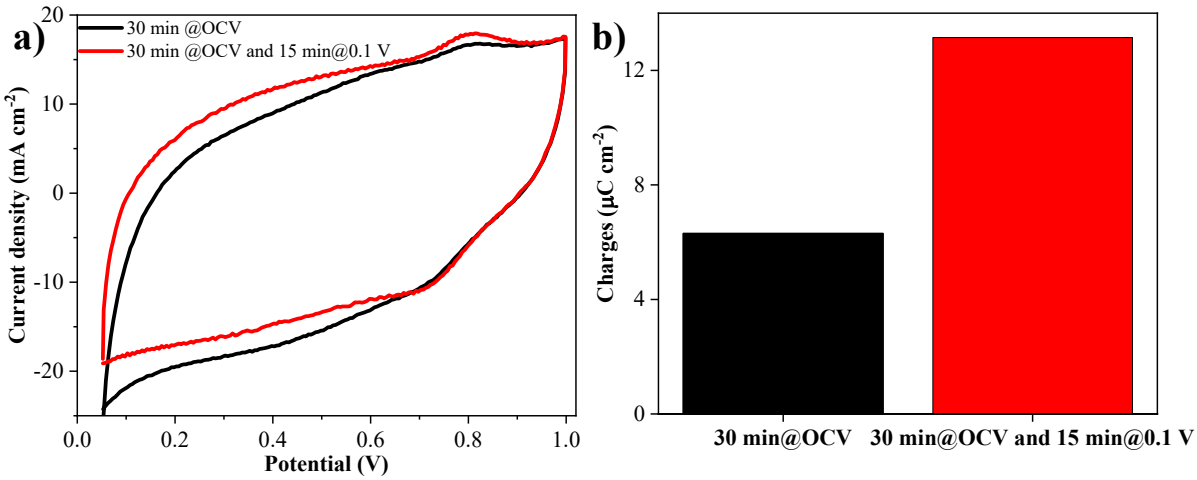

Supplementary Fig. 13 Cyclic voltammetry in H_2/N_2, **a** After 30 mins at OCV (black), and 30 mins at OCV followed by 15 mins @ 0.1 V (red), **b** Corresponding charges of the Fe(II)/Fe(III) redox transition peak.

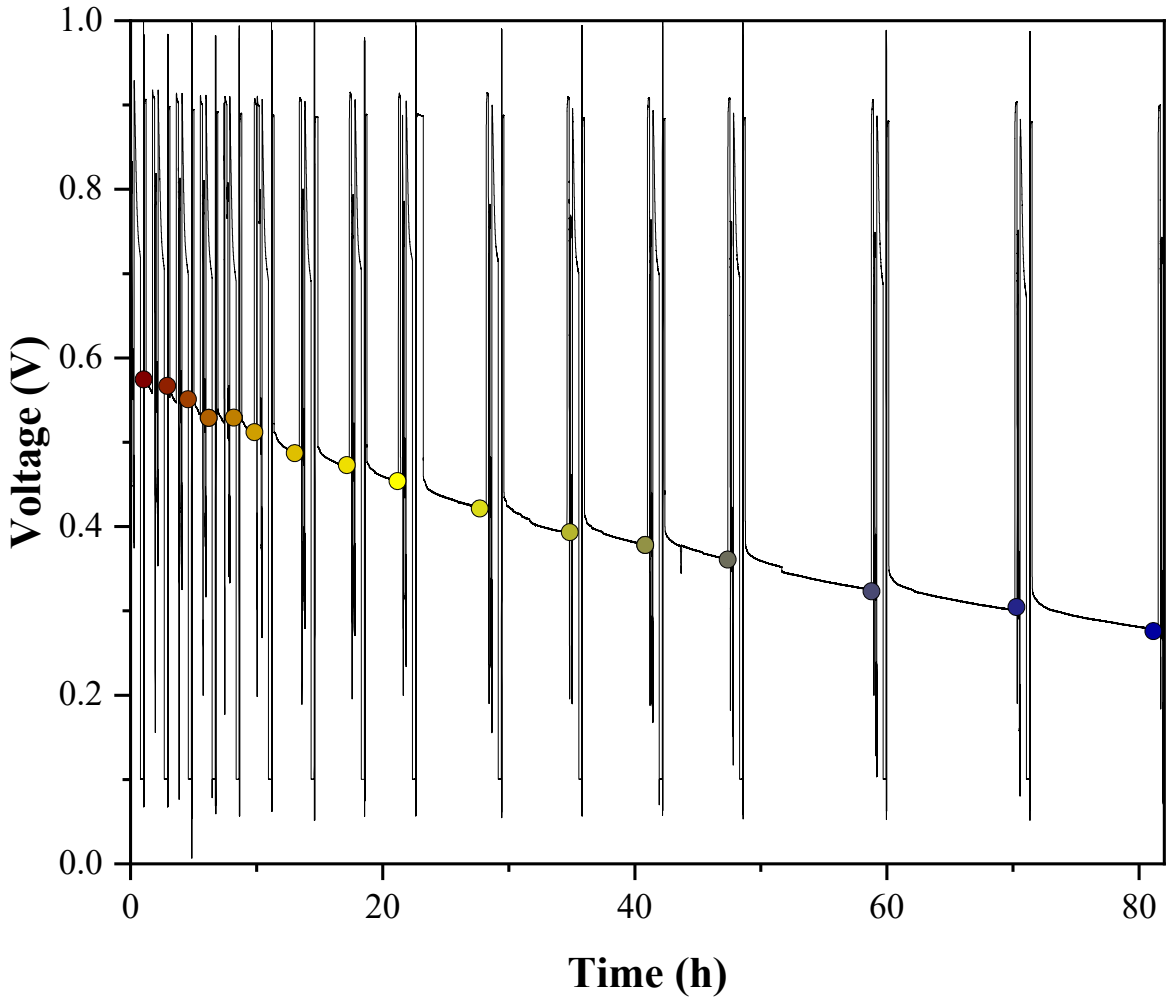

Supplementary Fig. 14 Performances over the 60 hours stability test with 16 intermediate measurement steps. The circles indicate the measurement steps, with the colours corresponding to the timestamps of Fig. 3b (e.g., the first circle corresponds to the test at 0h test, and the last circle to 60 hours).

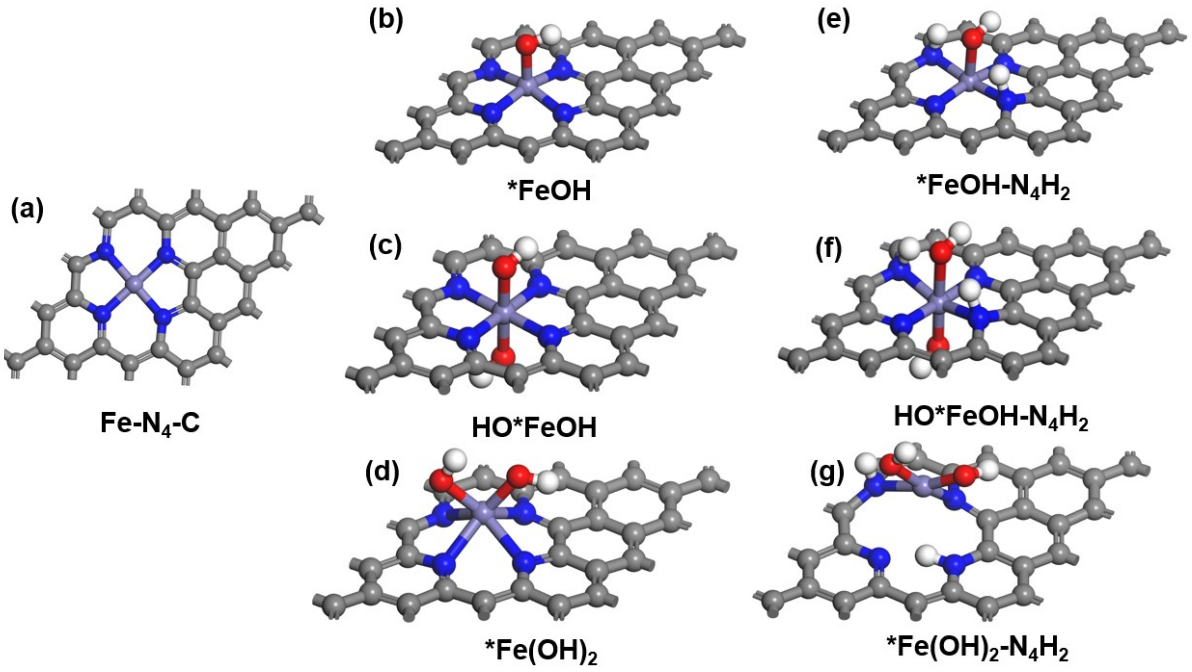

Supplementary Fig. 15 a DFT optimized structure of Fe-N_4-C catalysts; **b-d** DFT optimized structures of Fe-N_4-graphene catalysts with different intermediates (*FeOH, HO*FeOH, and *$Fe(OH)_2$) during oxygen reduction reaction (ORR); **e-f** DFT optimized structures with 2 N protonation on Fe-N_4-C catalysts during ORR.

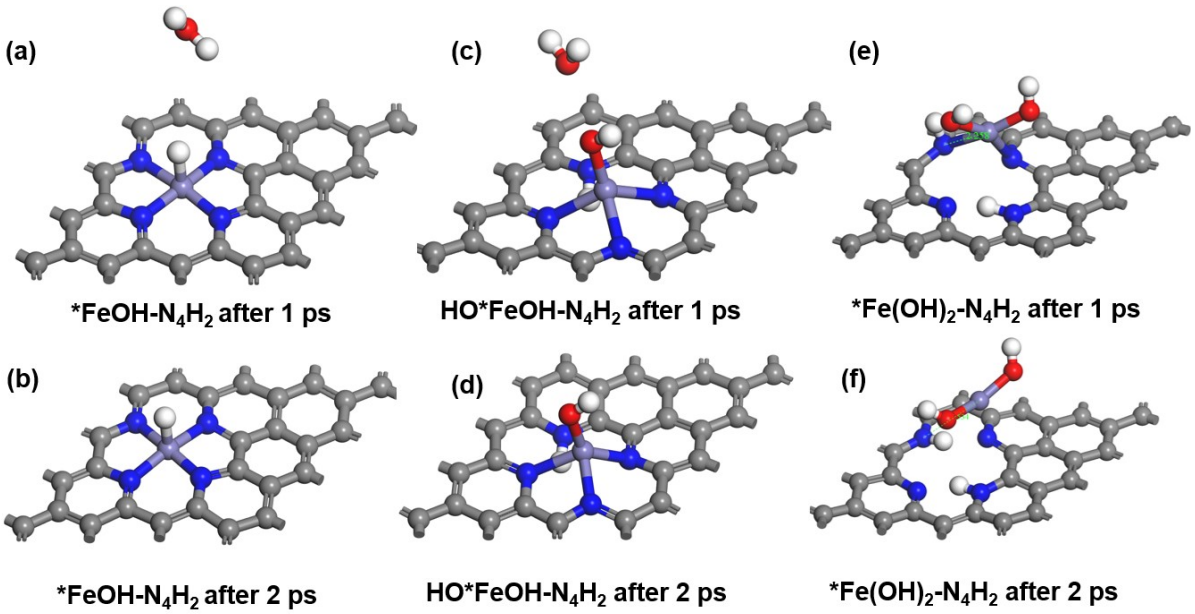

Supplementary Fig. 16. AIMD optimized configurations of *FeOH, HO*FeOH, and *$Fe(OH)_2$ intermediates with N protonation in FeNC catalysts. **a** *FeOH-N_4H_2 after 1 ps and **b** 2 ps; **c** HO*FeOH-N_4H_2 after 1 ps and **d** 2 ps; **e** *$Fe(OH)_2$-N_4H_2 after 1 ps and **f** 2 ps. ps : picosecond.

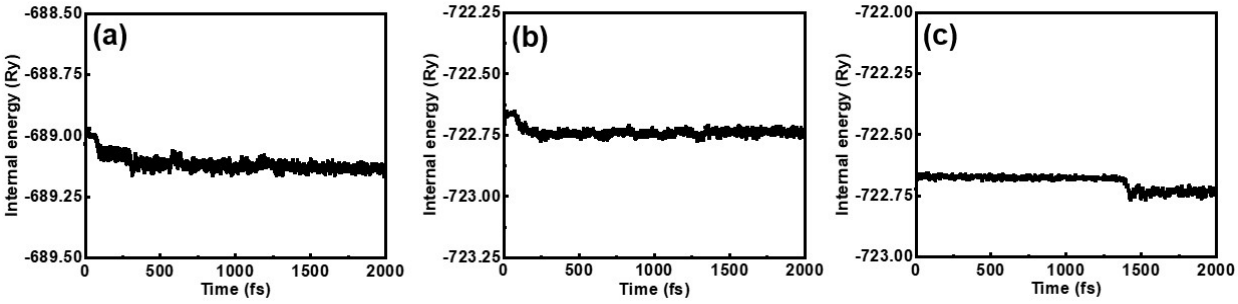

Supplementary Fig. 17. Internal energies of **a** *FeOH, **b** HO*FeOH, and **c** *$Fe(OH)_2$ intermediates with N protonation on FeNC catalysts within 2 ps AIMD simulation.

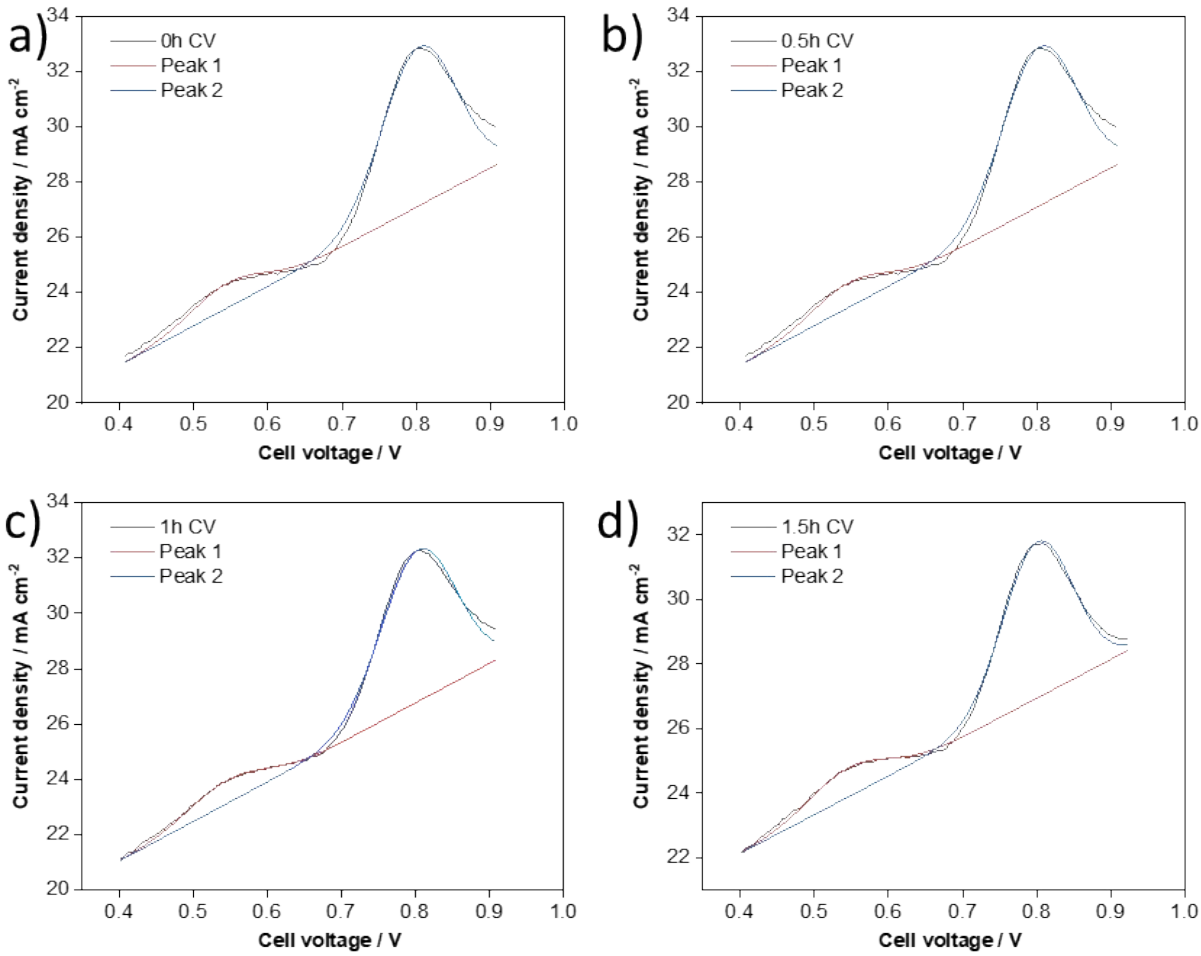

Supplementary Fig. 18 Fitted oxidation part of the cyclic voltammograms in H_2/N_2 from 0.4 to 0.9 V after **a** 0h, **b** 0.5h, **c** 1h and **d** 1.5h of stability tests at 1 A cm^{-2} for Fe-N-C PEMFC.

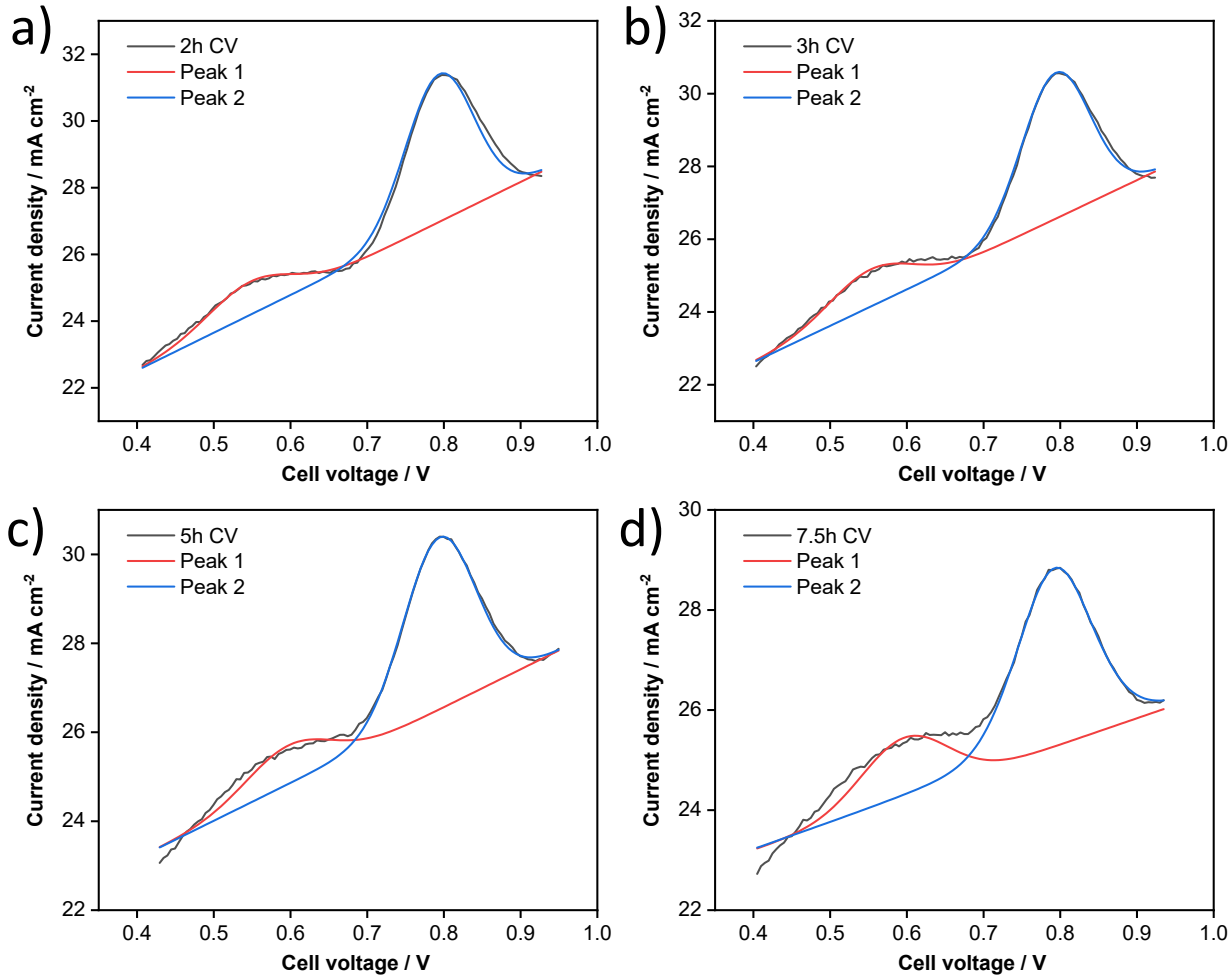

Supplementary Fig. 19 Fitted oxidation part of the cyclic voltammograms in H_2/N_2 from 0.4 to 0.9 V after **a** 2h, **b** 3h, **c** 5h and **d** 7.5h of stability tests at 1 A cm^{-2} for Fe-N-C PEMFC.

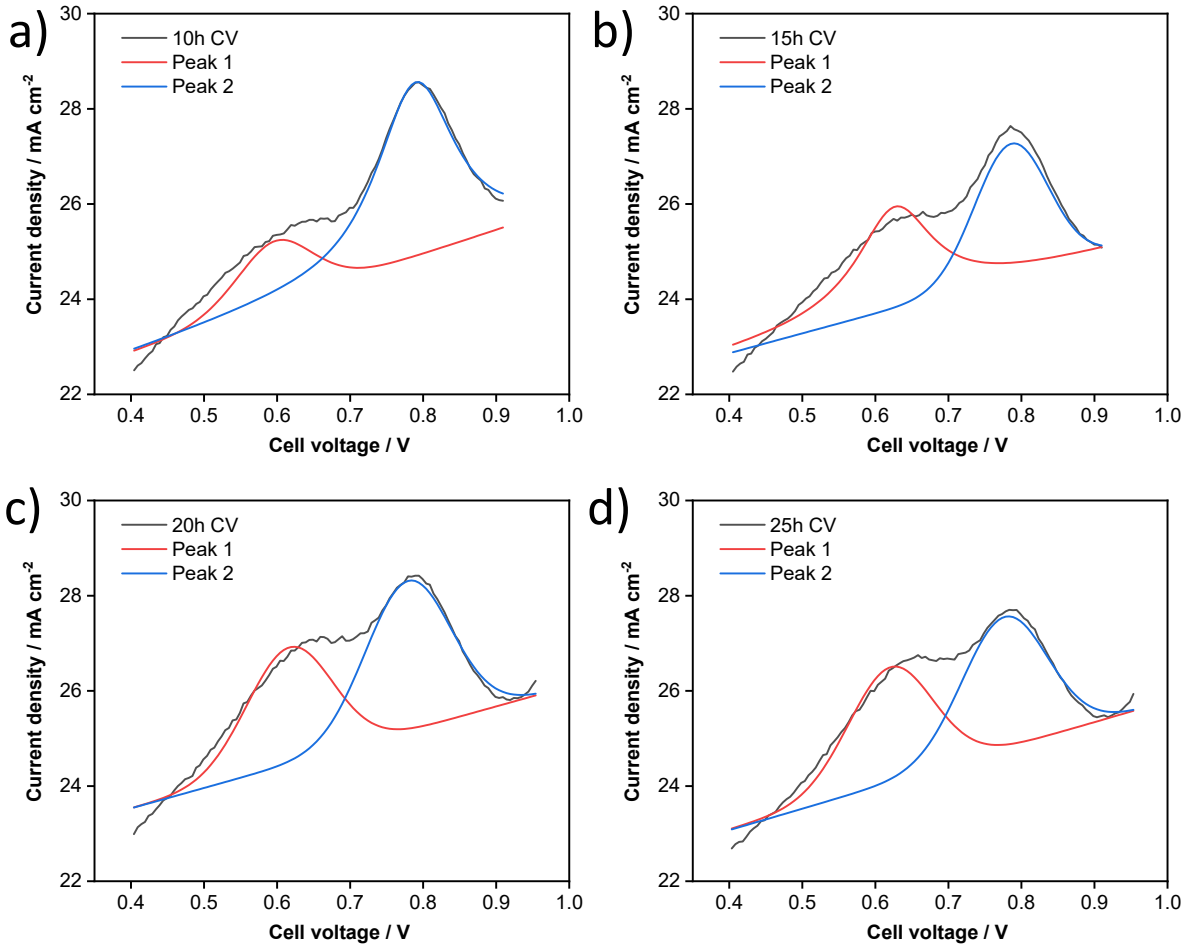

Supplementary Fig. 20 Fitted oxidation part of the cyclic voltammograms from 0.4 to 0.9 V after **a** 10h, **b** 15h, **c** 20h and **d** 25 h of stability tests at 1 A cm^{-2} for Fe-N-C PEMFC in H_2/N_2.

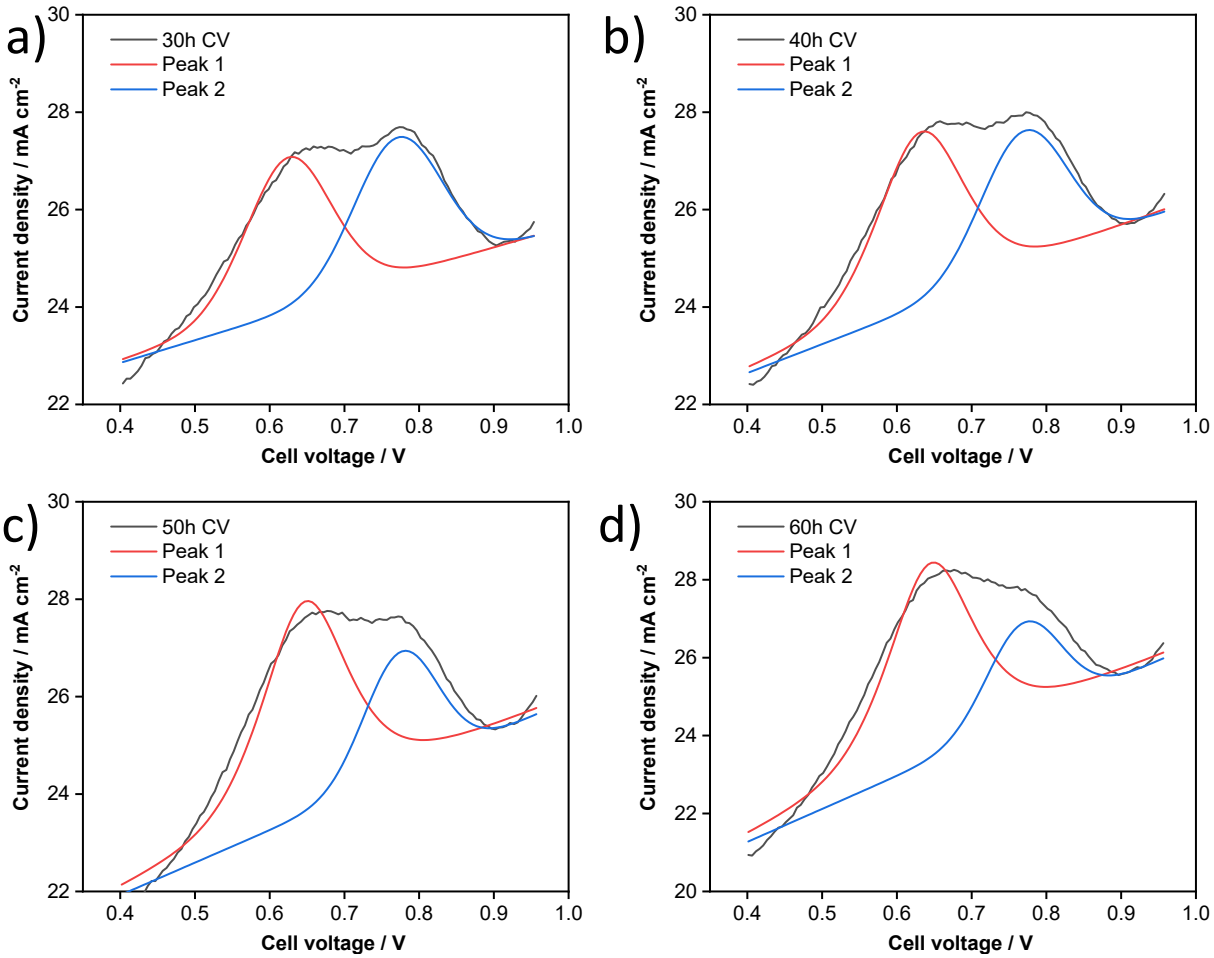

Supplementary Fig. 21 Fitted oxidation part of the cyclic voltammograms from 0.4 to 0.9 V after **a** 30h, **b** 40h, **c** 50h and **d** 60h of stability tests at 1 A cm^{-2} for Fe-N-C PEMFC in H_2/N_2.

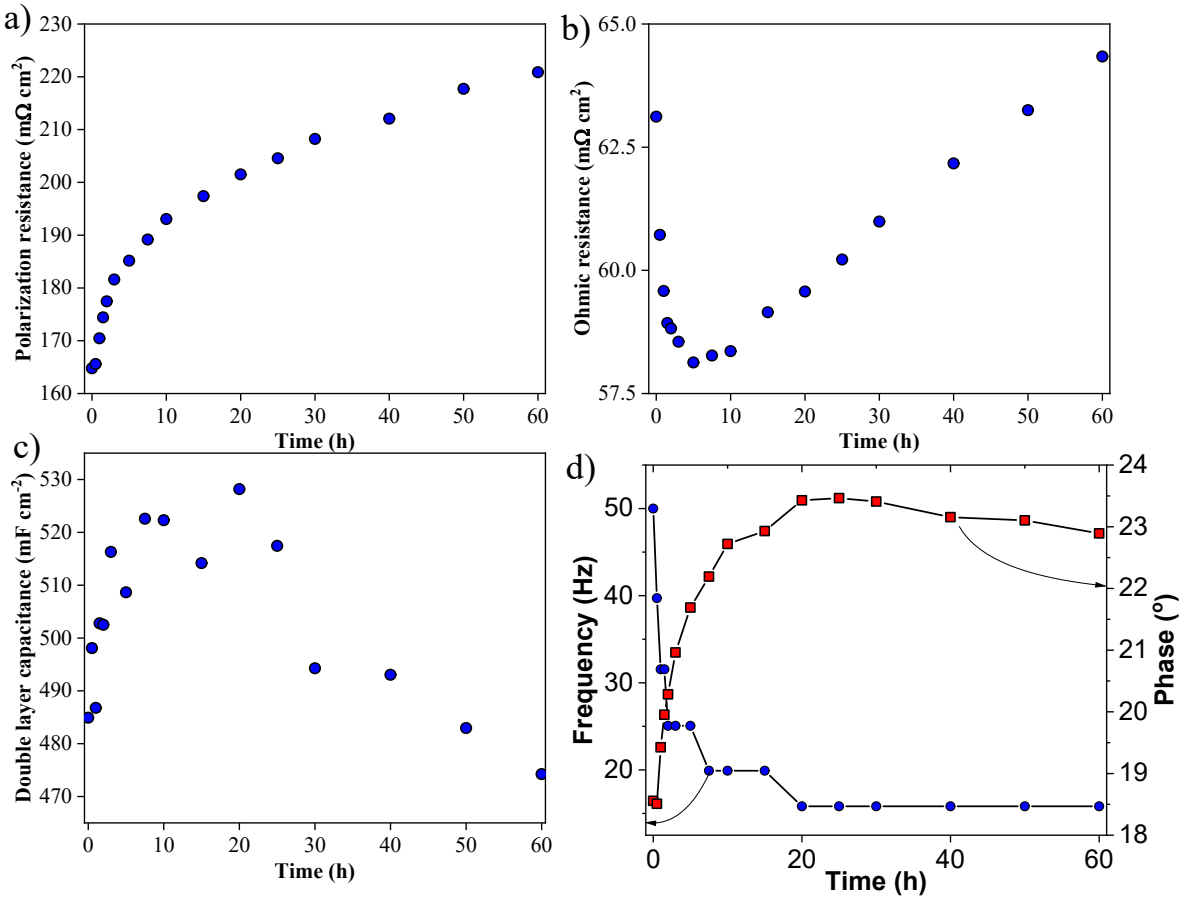

Supplementary Fig. 22 a Polarization resistance and **b** ohmic resistance at 1 A cm^{-2} through the 60 hours stability test captured using impedance. **c** Double-layer capacitance obtained from cyclic voltammetry. **d** Phase shift and frequency reduction at the EIS semi-circle peak obtained from Nyquist plots.

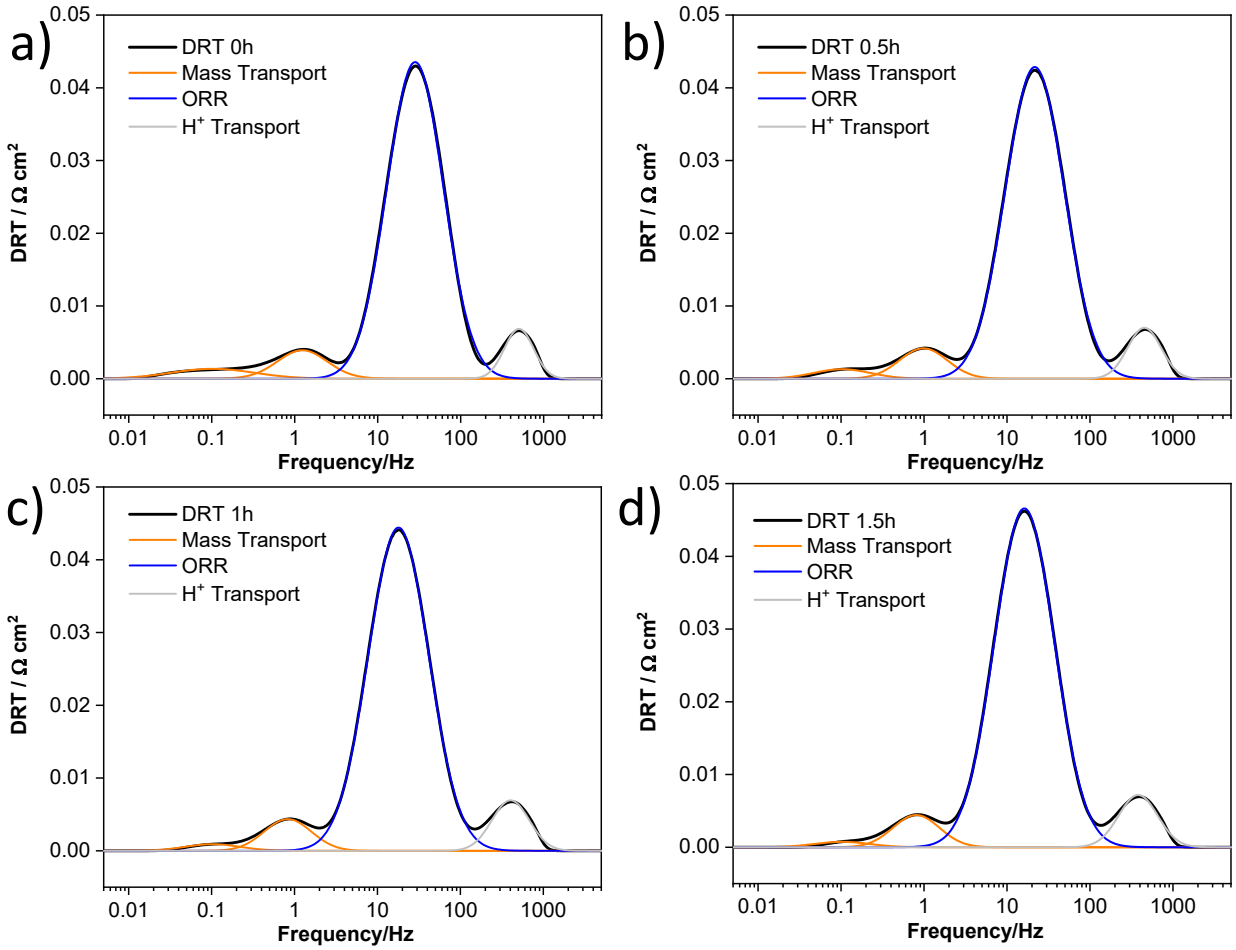

Supplementary Fig. 23 DRT fits for EIS results after **a** 0h, **b** 0.5h, **c** 1h and **d** 1.5 h at 1 A cm^{-2}.

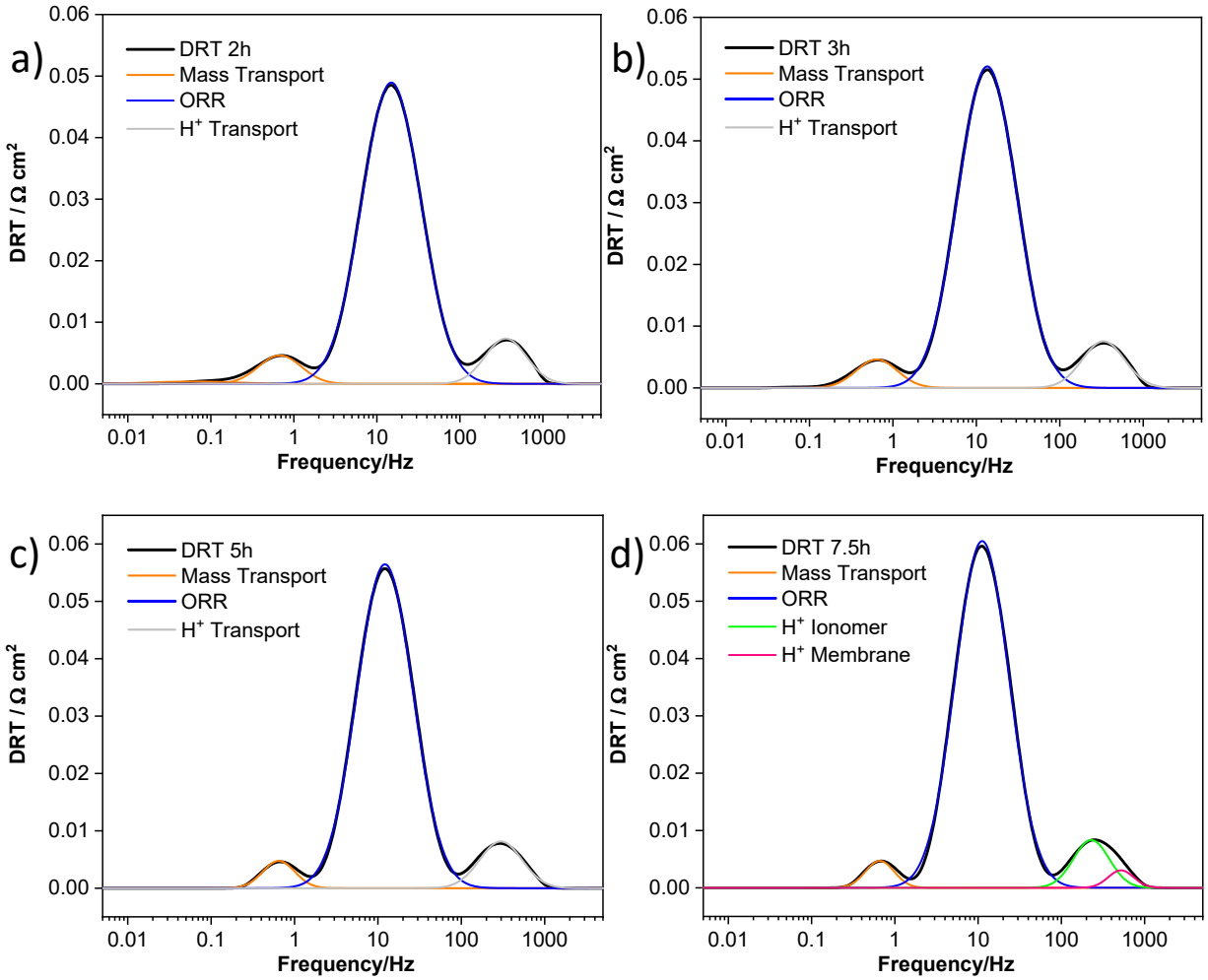

Supplementary Fig. 24 DRT fits for EIS results after **a** 2h, **b** 3h, **c** 5h and **d** 7.5 h at 1 A cm^{-2}.

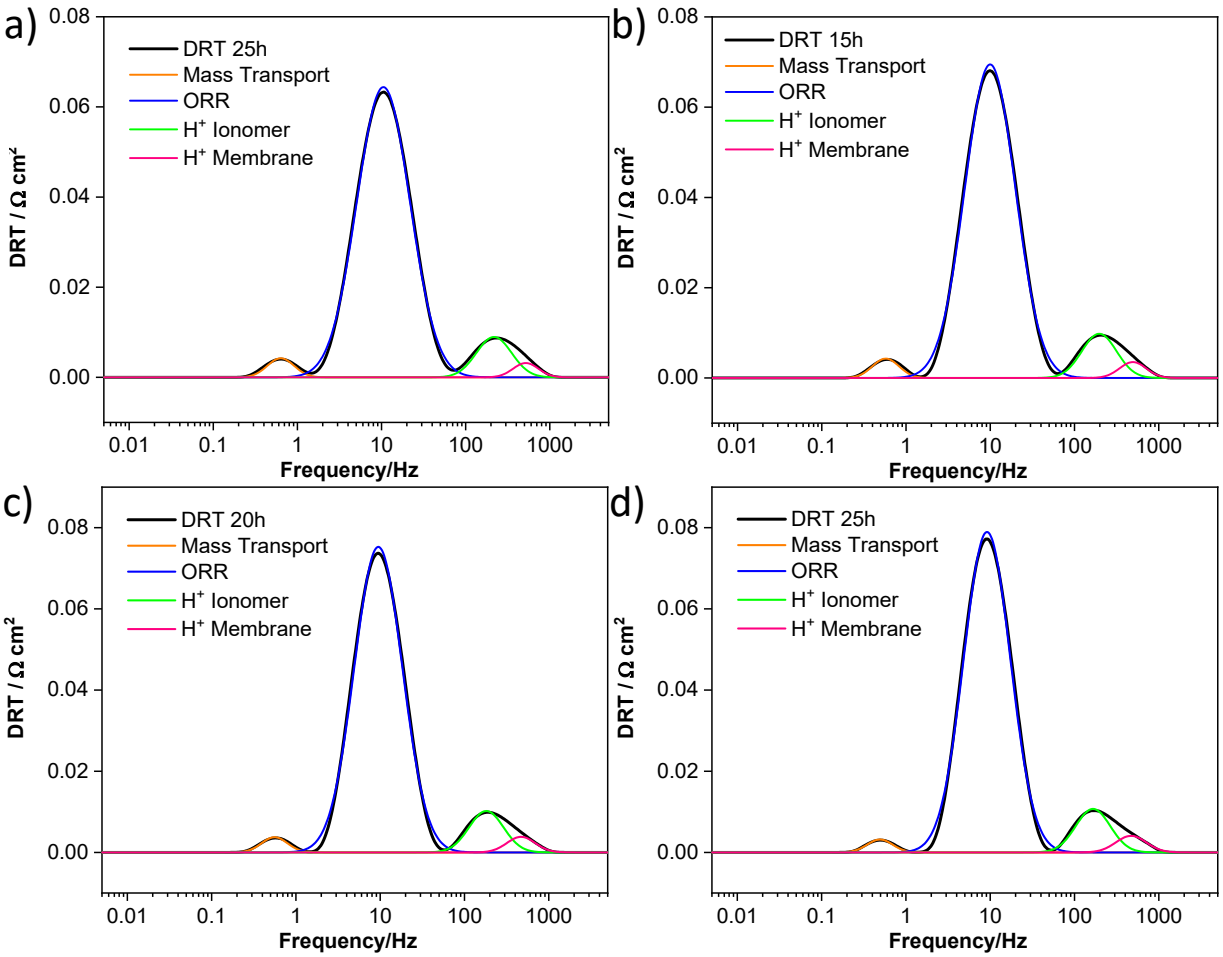

Supplementary Fig. 25 DRT fits for EIS results after **a** 10h, **b** 15h, **c** 20h and **d** 25 h at 1 A cm^{-2}.

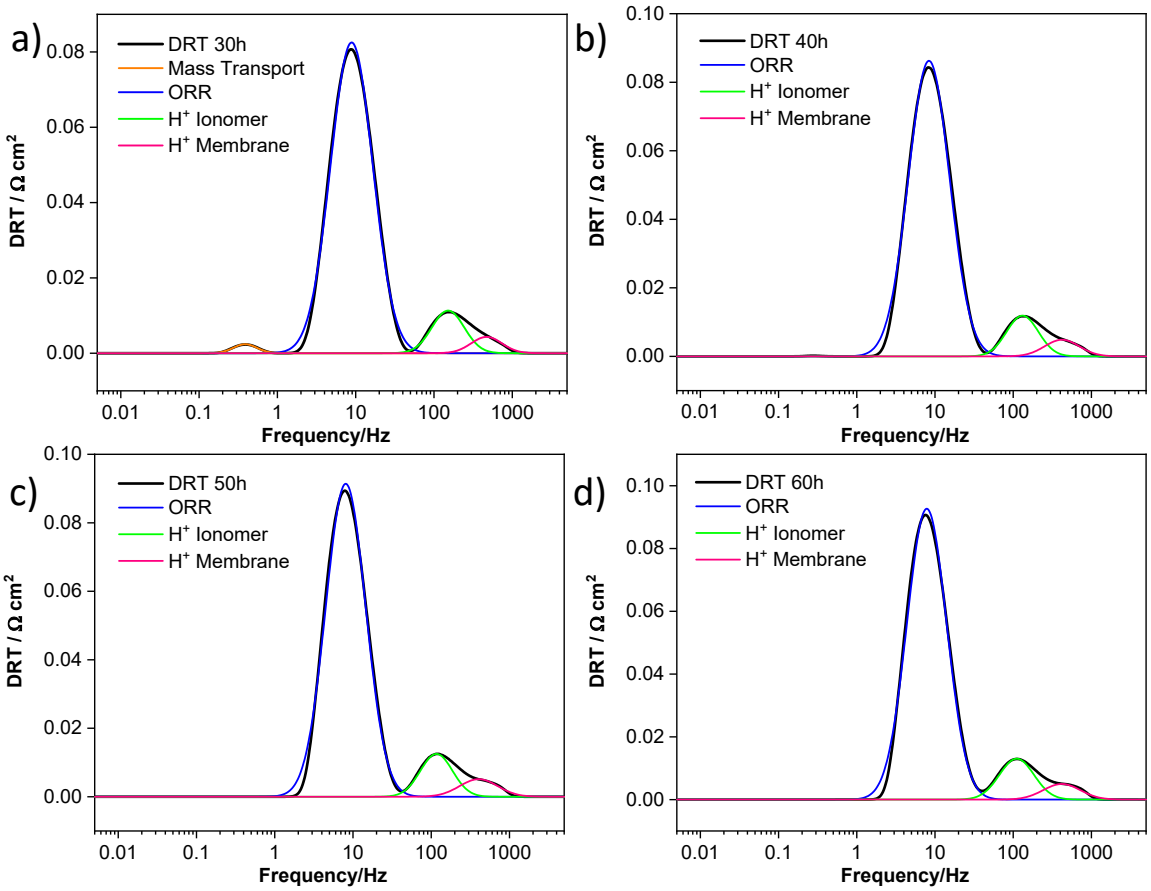

Supplementary Fig. 26 DRT fits for EIS results after **a** 30h, **b** 40h, **c** 50h and **d** 60 h at 1 A cm^{-2}

Note: While EIS measurements are carried out from 5 kHz to 0.1 Hz, the DRT software from the Ciucci group[4] has predictive capabilities towards lower frequencies (5 mHz), which were not considered in this analysis. Specifically, the low-frequency DRT peak from ~10 mHz to ~0.5 Hz, present from 0 to 3h was not considered in the analysis.

Supplementary Table 1. Overview of PGM-free catalysts performances and stability in low-temperature PEMFCs.

Catalysts	Configuration	Loading (mg cm^{-2})	Power density (W cm^{-2})	Open circuit voltage (V)	Half-wave potential (V versus RHE)	Onset potential (V versus RHE)	Performance loss	Refs
CoNC-ArNH_3	Co-N_4	3	0.44 (O_2)/0.21 (Air)	0.88 (Air)	0.785	0.89	65% in 20 h at 0.4 V	[14]
20Co-NC-1100	Co-N_4	4	0.56 (O_2)/0.28 (Air)	0.95 (O_2)	0.80	0.93	55% in 100 h at 0.7 V	[15]
Co@SACo-N-C	Co-N_x	4	0.42 (O_2)/0.23 (Air)	0.91 (O_2)	0.778	0.925	16% in 100 h at 0.3 A cm^{-2}	[16]
20Mn-NC-second	Mn-N_4	4	0.46(O_2)	0.95 (O_2)	0.80	-	22.5% in 100 h at 0.7 V	[17]
Fe2-Z8-C	Fe-N_4	2.8	1.14 (O_2)	1 (O_2)	0.805	0.902	85% in 50 h at 0.5 V	[18]
TPI@Z8(SiO_2)-650-C	Fe-N_4	2.7	1.18 (O_2)	0.91 (Air)	0.823	-	80% in 50 h at 0.5 V	[19]
Fe/N/C(4mIm)-OAc-2bar	Fe-N_4	3	1.33 (O_2)	1 (O_2)	-	-	80.3% in 35 h at 0.5 V	[20]
Fe_g–NC/Phen	Fe-N_4	3.5	1.53 (O_2)	0.95	0.84	0.9	85% in 25 h at 0.6 V	[21]
Fe-N-C	Fe-N_4	3	0.93	0.97 (O_2)	0.81	0.90	52% in 60 h at 1 A cm^{-2}	This work
C-FeHZ8@g-C_3N_4-950	Fe-N_4	4	0.628(O_2)	0.98(O_2)	0.78	-	50.3% in 8 h at 0.7 V	[22]
FeN_4/HOPC-c-1000	Fe-N_4	4	0.66 (O_2)/0.42 (Air)	0.99(O_2)	0.80	0.90	47% in 100 h at 0.55 V	[23]
1.5Fe-ZIF	Fe-N_4	4	0.66 (O_2)/0.36 (Air)	0.98(O_2)	0.88	-	40% in 100 h at 0.7 V	[24]
Fe_{SA}/Fe_{AC}–2DNPC	Fe-N4	1.5	0.94 (O_2)	0.92 (O_2)	0.81 V	-	23% in 150 h at 0.5 V	[25]
Fe-AC-CVD	Fe-N_4	4	0.56 (Air)	0.92 (Air)	0.816	0.9	13% in 317 h at 0.67 V	[26]
Fe-N-C CVD-750	Fe-N_4	6	0.37 (Air)	0.95 (Air)	0.85	0.9	-	[27]

The numbers in the 4th to 9th column were either reported in the cited papers or measured from the papers charts for this table creation.

Supplementary Table 2. C, N, O, and Fe contents in the N-C and Fe-N-C determined by XPS measurements.

Sample	N-C	Fe-N-C
C 1s (at%)	90.43	82.21
N 1s (at%)	5.72	5.20
O 1s (at%)	3.06	10.50
Fe 2p (at%)	-	2.09
Zn 2p (at%)	0.79	-

Supplementary Table 3. Physical constants (at 1 bar, 25 °C) and cell constants to calculate the H_2O_2 generated over 60 hours.

Parameter	Value
Applied current, I / A	1
H_2O_2 yield at 80 °C, x / %	4 to 5
Stability test duration, Δt / s	60×3600
Faraday's constant, F / C mol^{-1}	96500
Catalyst loading, L / mg cm^{-2}	3
4 electron pathways, $n_e(H_2O)$	4
2-electron pathways, $n_e(H_2O_2)$	2
Amount of H_2O_2 generated over the stability test, $N_{H_2O_2}$/ mol mg^{-1}	0.18 to 0.95 $\times 10^{-3}$

3. Matlab Code for the 3D-DRT graph.

```
X=[] % frequency data as a single column
Y=[0.1 0.5 1 1.5 2 3 5 7.5 10 15 20 25 30 40 50 60]; % This corresponds to each current density.
Z=[]; % input the DRT results in a column table with the same length as X and width as Y.
X1=[]; %in X1 input an array the same length as X, but with 1 in every line.
surf(Y,X,Z)
hold on
plot3(X1*0.1,X,Z1(:,1),'k','LineWidth',1.1);
plot3(X1*0.5,X,Z1(:,2),'k','LineWidth',1.1);
plot3(1*X1,X,Z1(:,3),'k','LineWidth',1.1);
plot3(1.5*X1,X,Z1(:,4),'k','LineWidth',1.1);
plot3(2*X1,X,Z1(:,5),'k','LineWidth',1.1);
plot3(3*X1,X,Z1(:,6),'k','LineWidth',1.1);
plot3(5*X1,X,Z1(:,7),'k','LineWidth',1.1);
plot3(7.5*X1,X,Z1(:,8),'k','LineWidth',1.1);
plot3(10*X1,X,Z1(:,9),'k','LineWidth',1.1);
plot3(15*X1,X,Z1(:,10),'k','LineWidth',1.1);
plot3(20*X1,X,Z1(:,11),'k','LineWidth',1.1);
plot3(25*X1,X,Z1(:,12),'k','LineWidth',1.1);
plot3(30*X1,X,Z1(:,13),'k','LineWidth',1.1);
plot3(40*X1,X,Z1(:,14),'k','LineWidth',1.1);
plot3(50*X1,X,Z1(:,15),'k','LineWidth',1.1);
plot3(60*X1,X,Z1(:,16),'k','LineWidth',1.1);
hold off
shading interp;
colorbar
colormap(jet);
set(gca, 'XScale', 'log')
set(gca, 'YScale', 'log')
set(gca, 'FontName', 'Arial')
set(gca, 'FontSize',15.5)
set(gca,'linewidth',1.25)
set(gca, 'YDir','reverse')
view([-80.662191780821914,41.399999999999999])
% set(gca,'ColorScale','log')
xticks([0.1 1 10 60])
xticklabels({'0','1h','10h','60h'}
.);
yticks([0.01 0.1 1 10 100 1000 5000])
yticklabels({'0.01','0.1','1','10','100','1k','5k'})
set (gca, 'ydir', 'reverse')
b=max(Z1(:));
xlim([0 60])
ylim([0.1 5000])
zlim([0 b+1])
caxis([0 b+1])
box on;
```

4. Supplementary References

1. V. Goellner, V. Armel, A. Zitolo, E. Fonda and F. Jaouen, *J. Electrochem. Soc.*, 2015, **162**, H403-H414.
2. Maxim, Peak fitting to either Voigt or LogNormal line shapes. , https://www.mathworks.com/matlabcentral/fileexchange/52321-peak-fitting-to-either-voigt-or-lognormal-line-shapes).
3. L. Zhou, Y. Li, X. Chen, Z. Yang, S. Yang, Q. Wang, X.-Y. Liu and S. Lu, *J. Mater. Chem. A*, 2022, **10**, 20323-20330.
4. F. Ciucci and C. Chen, *Electrochim. Acta*, 2015, **167**, 439-454.
5. T. H. Wan, M. Saccoccio, C. Chen and F. Ciucci, *Electrochim. Acta*, 2015, **184**, 483-499.
6. M. Heinzmann, A. Weber and E. Ivers-Tiffée, *J Power Sources*, 2018, **402**, 24-33.
7. Q. Meyer, S. Liu, Y. Li and C. Zhao, *J. Power Sources*, 2022, **533**, 231058.
8. Q. Meyer, N. Mansor, F. Iacoviello, P. L. Cullen, R. Jervis, D. Finegan, C. Tan, J. Bailey, P. R. Shearing and D. J. L. Brett, *Electrochim. Acta*, 2017, **242**, 125-136.
9. P. Giannozzi, S. Baroni, N. Bonini, M. Calandra, R. Car, C. Cavazzoni, D. Ceresoli, G. L. Chiarotti, M. Cococcioni, I. Dabo, A. Dal Corso, S. de Gironcoli, S. Fabris, G. Fratesi, R. Gebauer, U. Gerstmann, C. Gougoussis, A. Kokalj, M. Lazzeri, L. Martin-Samos, N. Marzari, F. Mauri, R. Mazzarello, S. Paolini, A. Pasquarello, L. Paulatto, C. Sbraccia, S. Scandolo, G. Sclauzero, A. P. Seitsonen, A. Smogunov, P. Umari and R. M. Wentzcovitch, *Journal of Physics: Condensed Matter*, 2009, **21**, 395502.
10. P. E. Blöchl, *Physical Review B*, 1994, **50**, 17953-17979.
11. B. Hammer, L. B. Hansen and J. K. Nørskov, *Physical Review B*, 1999, **59**, 7413-7421.
12. N. Yang, L. Peng, L. Li, J. Li, Q. Liao, M. Shao and Z. Wei, *Chemical Science*, 2021, **12**, 12476-12484.
13. Y. Yang, J. Li, C. Zhang, Z. Yang, P. Sun, S. Liu and Q. Cao, *The Journal of Physical Chemistry C*, 2022, **126**, 4338-4346.
14. L. Chen, X. Liu, L. Zheng, Y. Li, X. Guo, X. Wan, Q. Liu, J. Shang and J. Shui, *Appl. Catal. B Environ.*, 2019, **256**, 117849.
15. X. X. Wang, D. A. Cullen, Y. T. Pan, S. Hwang, M. Wang, Z. Feng, J. Wang, M. H. Engelhard, H. Zhang, Y. He, Y. Shao, D. Su, K. L. More, J. S. Spendelow and G. Wu, *Adv. Mater.*, 2018, **30**, 1-11.
16. Q. Cheng, S. Han, K. Mao, C. Chen, L. Yang, Z. Zou, M. Gu, Z. Hu and H. Yang, *Nano Energy*, 2018, **52**, 485-493.
17. J. Li, M. Chen, D. A. Cullen, S. Hwang, M. Wang, B. Li, K. Liu, S. Karakalos, M. Lucero, H. Zhang, C. Lei, H. Xu, G. E. Sterbinsky, Z. Feng, D. Su, K. L. More, G. Wang, Z. Wang and G. Wu, *Nat. Cat.*, 2018, **1**, 935-945.
18. Q. Liu, X. Liu, L. Zheng and J. Shui, *Angew. Chem. Int. Ed.*, 2018, **57**, 1204-1208.
19. X. Wan, X. Liu, Y. Li, R. Yu, L. Zheng, W. Yan, H. Wang, M. Xu and J. J. N. C. Shui, *Nat. Catal.*, 2019, **2**, 259-268.
20. Y. Li, P. Zhang, L. Wan, Y. Zheng, X. Qu, H. Zhang, Y. Wang, K. Zaghib, J. Yuan, S. Sun, Y. Wang, Z. Zhou and S. Sun, *Adv. Funct. Mater.*, 2021, **31**, 2009645.
21. S.-H. Yin, S.-L. Yang, G. Li, G. Li, B.-W. Zhang, C.-T. Wang, M.-S. Chen, H.-G. Liao, J. Yang, Y.-X. Jiang and S.-G. Sun, *Energy Environ. Sci.*, 2022, **15**, 3033-3040.
22. Y. Deng, B. Chi, X. Tian, Z. Cui, E. Liu, Q. Jia, W. Fan, G. Wang, D. Dang, M. Li, K. Zang, J. Luo, Y. Hu, S. Liao, X. Sun and S. Mukerjee, *J. Mater. Chem. A*, 2019, **7**, 5020-5030.
23. M. Qiao, Y. Wang, Q. Wang, G. Hu, X. Mamat, S. Zhang and S. Wang, *Angew. Chem. Int. Ed.*, 2020, **59**, 2688-2694.

24. H. Zhang, H. T. Chung, D. A. Cullen, S. Wagner, U. I. Kramm, K. L. More, P. Zelenay and G. Wu, *Energy Environ. Sci.*, 2019, **12**, 2548-2558.
25. X. Wan, Q. Liu, J. Liu, S. Liu, X. Liu, L. Zheng, J. Shang, R. Yu and J. Shui, *Nat. Commun.*, 2022, **13**, 2963.
26. S. Liu, C. Li, M. J. Zachman, Y. Zeng, H. Yu, B. Li, M. Wang, J. Braaten, J. Liu, H. M. Meyer, M. Lucero, A. J. Kropf, E. E. Alp, Q. Gong, Q. Shi, Z. Feng, H. Xu, G. Wang, D. J. Myers, J. Xie, D. A. Cullen, S. Litster and G. Wu, *Nat. Energy*, 2022, **7**, 652-663.
27. L. Jiao, J. Li, L. L. Richard, Q. Sun, T. Stracensky, E. Liu, M. T. Sougrati, Z. Zhao, F. Yang, S. Zhong, H. Xu, S. Mukerjee, Y. Huang, D. A. Cullen, J. H. Park, M. Ferrandon, D. J. Myers, F. Jaouen and Q. Jia, *Nat. Mater.*, 2021, DOI: https://doi.org/10.1038/s41563-021-01030-2, 1-9.